3-2006

Some Aspects of the Mechanical Response of BMI 5250-4 Neat Resin at 191°C: Experiment and Modeling

John G. Balaconis

SOME ASPECTS OF THE MECHANICAL RESPONSE OF BMI 5250-4 NEAT RESIN AT 191ºC: EXPERIMENT AND MODELING

THESIS

John G. Balaconis, 2nd Lt, USAF

AFIT/GAE/ENY/06-M03

DEPARTMENT OF THE AIR FORCE
AIR UNIVERSITY

AIR FORCE INSTITUTE OF TECHNOLOGY

Wright-Patterson Air Force Base, Ohio

The views expressed in this thesis are those of the author and do not reflect the official policy or position of the United States Air Force, Department of Defense, or the U.S. Government.

AFIT/GAE/ENY/06-M03

SOME ASPECTS OF THE MECHANICAL RESPONSE OF BMI 5250-4 NEAT RESIN AT 191ºC: EXPERIMENT AND MODELING

THESIS

Presented to the Faculty

Department of Aeronautics and Astronautics

Graduate School of Engineering and Management

Air Force Institute of Technology

Air University

Air Education and Training Command

In Partial Fulfillment of the Requirements for the

Degree of Master of Science in Aeronautical Engineering

John G. Balaconis, BS

2nd Lt, USAF

March 2006

AFIT/GAE/ENY/06-M03

SOME ASPECTS OF THE MECHANICAL RESPONSE OF BMI 5250-4 NEAT RESIN AT 191ºC: EXPERIMENT AND MODELING

John G. Balaconis, BS

2nd Lt, USAF

Approved:

/signed/

Dr. Marina Ruggles-Wrenn (Chairman)	Date

/signed/

Dr. Greg A. Schoeppner (Member)	Date

/signed/

Dr. Richard B. Hall (Member)	Date

Abstract

The mechanical response of BMI 5250-4 neat resin at 191ºC was studied using both creep and recovery tests where several variables were allowed to change. In these tests, the effect of stress rate, prior history, and panel variability were all taken into account. During the creep test, the material showed both primary and secondary creep over 20 h. The recovery tests showed full recovery after it was subjected to 80% UTS. The higher stress rate caused a much greater response in both creep and recovery tests. The prior history was studied by allowing the specimens to go through a stepwise creep test. They behaved similar to the single step creep test when preceded by a loading segment. During creep tests preceded by unloading, the material showed a decrease in creep strain. This decrease grew as the creep stress approached zero. The only difference that could be seen with panel variability was that the UTS dropped dramatically between the panels.

A nonlinear viscoelastic model was created that was based on the work by Schapery. This model included four constants that were material specific and stress dependant. These constants were obtained by viewing the response during a two- step loading program including creep and recovery. The model was verified by comparing the predictions to previous tests including the creep and stepwise creep tests. The model predicted the creep strain preceded by loading well. It was capable of showing the response of the negative creep but the error grew as more steps were introduced. The model could not take into account stress rate. Therefore it could only predict the results at the higher stress rate.

Acknowledgments

I would like to thank the following people who gave both their time and expertise to make this process go as smooth as possible: my thesis advisor, Dr. Marina Ruggles-Wrenn, for all the advice and resources that she made available to me, Ms. Thao Gibson (AFRL/ML), for showing me the step by step process to creating BMI 5250-4, Dr. Greg Schoeppner (AFRL/MLBCM), Dr. Charles Y-C Lee (AFOSR/NE), and Dr. Richard Hall (AFRL/MLBCM) for their sponsorship of my thesis, Barry Page, Andy Pitts, and Jay Anderson, for the setup and maintenance of everything in the lab, and to Captain John Mehrman and 2Lt Patrick Jackson, for keeping me on track.

John G. Balaconis

Table of Contents

Page

Page

List of Figures

Figure **Page**

Page

Page

List of Tables

Table **Page**

SOME ASPECTS OF THE MECHANICAL REPONSE OF BMI 5250-4 AT 191ºC: EXPERIMENT AND MODELING

I. Introduction

The benefits of composites have been known to the world for thousands of years. There were biblical references made about mud bricks that were reinforced with straw in Ancient Egypt (5:4). Since that time, their capabilities have been improved in numerous ways.

Composites can be divided into three groups depending on their matrix material. These three groups include polymers, ceramics, and metal. Each group has distinct properties that make them more suitable for certain applications. The polymer's main advantages include a low density and corrosion resistance.

These advantages make polymer composites very attractive to the aerospace industry. They have appeared in planes as early as World War II (2:435). Since that time, there have been vast improvements in both the knowledge and manufacturing capabilities that have allowed polymers to have a more prominent place in engineering design. They have slowly moved from secondary parts to primary load bearing structures. Polymers are even making a move into the engine as their temperature capabilities continue to improve. As time goes on, the use of polymers in aerospace applications will only grow.

There are numerous modeling methods available to engineers today. They are important in that they allow the engineer to get an idea of how the material will respond under certain conditions without going through numerous tests. As the accuracy of these models improves, the more complex the equations become. There are methods available that can take into account such variables as temperature, load rates, and even prior history.

In the following sections, all the steps taken in this research will be explained in great detail. It will begin with a background of all the information that was used in completing this research. It will discuss everything from basic composite information to the complex equations of the model. Next, it will discuss the material and how it went from the uncured resin to a test specimen. Following that section will be a discussion of all the test equipment used and what tests were performed on the specimen. The majority of the paper will discuss the results of all the tests. The final section will summarize everything and give recommendations for future works.

II. Background

This section presents a basic definition of a composite material and discusses the advantages composites offer over monolithic materials. Next, polymer composites are discussed, including the processing methods and their most common uses in the aerospace industry. In addition, basic concepts of the viscoelastic theory are introduced. Mechanical behavior of polymers and modeling of polymer deformation response using linear and nonlinear viscoelastic constitutive approaches are discussed. Finally, previous work on properties and response of high-temperature polymers is discussed and objectives of this research effort are outlined.

Composites

Due to their many benefits, composites are being used more and more in the manufacturing world. By definition, "a composite is material system consisting of two or more phases on a macroscopic scale, whose mechanical performance and properties are designed to be superior to those of the constituent materials acting independently" (5:3). The two major phases of a composite are the matrix and the reinforcement.

Different types of reinforcement can be used. In low performance composites, the reinforcement is usually in the form of short fibers (or whiskers) that provide a stiffening effect for the matrix. In high performance composites, the reinforcement is generally a continuous fiber. It forms the backbone of the composite and provides much of the strength. An important parameter that determines the strength of the composite is the volume fraction of reinforcement. This parameter provides information on how many

fibers are used and how well they are dispersed throughout the matrix. Higher fiber volume fractions obviously results in a stronger composite. The dispersion is also important. If the fibers are packed very close together, the composite is vulnerable to fracture in the weaker areas (5:4).

The matrix can have two different functions depending on the type of composite. In low performance composites, the matrix is the main load bearing item. It has a much different role in high performance composites. Due to the presence of the continuous fibers, it is not needed as a primary load bearer. Therefore, it is used to protect the fibers from corrosion and heat as well as transfer the load from fiber to fiber. This structural make-up gives composites several advantages over their monolithic material counterparts.

Polymers

Composite materials can be divided into three groups based on the matrix material. The three major groups are ceramics, metal, and polymers. Each group has certain properties which make them suitable for different applications in the engineering world.

A polymer is defined as "a substance composed of molecules which have long sequences of one or more species of atoms or groups of atoms linked to each other by primary, usually covalent, bonds" (15:3). The most common way of classifying polymers is by dividing them into three groups: thermoplastics, elastomers, and thermosets. Thermoplastics can be divided even further into crystalline and amorphous. This classification (see Figure 1) is popular in the engineering world because it is based on the molecular structure of the polymer (15:10).

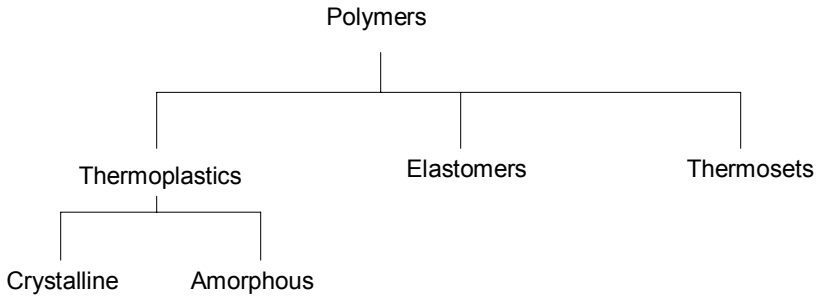

Figure 1. Polymer Classification Tree

Thermoplastics are often referred to as plastics and make up the largest group of polymers used in industry. These polymers have either a branched or linear skeletal structure, which means that their molecular chains can either be a single straight chain or include segments that branch out like branches of a tree. A great advantage of plastics is that they can be reshaped provided enough heat is applied. As mentioned earlier, the plastics can be divided into two groups: crystalline and amorphous. These polymers differ in the way that their molecular chains arrange themselves upon cooling. Each group has a unique property unto itself when it comes to temperature characteristics. The amorphous group, the bigger of the two, is characterized by a glass transition temperature (T_g). At this temperature, the material goes from a hard glass state to a rubbery soft state. At this state, the chains are allowed to move freely. The crystalline polymers on the other hand are characterized by a melting temperature (T_m) (12:31;15:10;25:18-19).

Elastomers are characterized by their cross linked skeletal structure. In this structure, molecular chains are attached to each other throughout the material. These polymers are unique from many other materials in that they can stretch to great lengths (3x to 10x their original size) and then quickly recover their original length when the load is released (15:11).

Thermosets can be described as network polymers with a high degree of cross linking among the molecular chains. Their main distinction is that unlike plastics, thermosets degrade instead of melting when heat is applied. Therefore these polymers can not be shaped over and over again (12:30-31;15:11). Thermosets include such materials as epoxy and bismaleimide resins (16:210).

Composite Fabrication

In today's manufacturing world, there are a number of ways of creating polymer composites. The process chosen depends on the necessary quality of the composite, cost, and the type of polymer used, such as a thermoset or a thermoplastic.

The first process used for fabricating composites with thermoset matrix was the wet lay-up method. First a layer of resin is laid out on a tool. At this point the fiber fabric is placed on top of the resin and absorbed into resin with the help of rolling. From there, resin is added until the desired thickness of the laminate is reached. This is a fairly simple process, however, it has numerous shortcomings, such as air bubbles trapped in the matrix and difficulty in controlling resin to fiber ratio. Furthermore this process is very labor-intensive and very messy. The said shortcomings resulted in materials that did not meet the standards required for today's aerospace applications (16:216).

Composites did not see much use in planes until the introduction of prepegs. "A prepreg is a material where the matrix resin has been impregnated into the fibers and is ready for immediate use" (16:216). In this process, the impregnated fibers are run through pinch rollers which remove air from the matrix and give the manufacturer better control over the resin to fiber ratio. Another advantage of this process is that the fibers can be held precisely in one direction throughout the matrix. This design allows engineers to fabricate the composites in a way that can best respond to the predicted load. From here, the process is still not complete. Laminates still need to be made. This can be accomplished in several different ways. Autoclave molding is the most popular method. In this process, the component is sealed in vacuum and placed in a pressurized oven. The pressure is raised to a required level, then the temperature is raised to cure the resin. When this step is completed, the temperature is lowered while the pressure remains constant until a safe temperature is reached (16:216-217).

Thermoplastics can be created in similar manners as their thermoset counterparts. One noticeable difference is that when preparing the laminates, each layer must be attached to the next by melting the resin in between them. Another important factor is that thermoplastics are very dependent on the cooling rate once the component has formed because this can affect the crystalline makeup that occurs in some plastics (16:221).

Aerospace Applications

Polymer composites can be found in aircrafts of all types from both the civilian and military sectors. They were first used in aircraft during World War II. Over time the manufacturing capabilities have improved in such a way that properties and cost of the

composite materials have made them more attractive to the aircraft industry. Composites offer unique advantages such as weight saving and corrosion protection that can not be obtained through monolithic metals.

The use of composites in civilian applications has been slow to develop. The reasons are due to the high cost of material certification as well as high manufacturing cost. Therefore, composites were used in secondary structures such as rudders and flaps. However, polymer composites have made recent strides toward primary structures in some large transports. One of the major developers in this movement is the Airbus Industrie. In the new Airbus A380, the wing carry-through structure will be made from a carbon-fiber-reinforced plastic composite. This single structure will have the dimension of 7 x 8 x 2.4 m. In all, about 16% of the aircraft total weight will be made of composite material. As manufacturing abilities continue to lower the cost of production, composites will be found more prominently in the civilian sector (2:436-438).

Military aircraft are at the other end of the spectrum when it comes to composite usage. The reason behind this diversity is that military aircraft are driven by performance more so than cost. Up to 70% of an airframe weight can be made of composites. Composites have been attractive because of their high stiffness, stealth abilities, and weight saving capabilities. In the recent design of the F-22, carbon/epoxy and carbon/BMI composites make up 24% of the aircraft weight (2:438-440;20:433).

Viscoelastic Behavior

Polymers have unique qualities that make them respond differently to certain loads than metals and/or ceramics. The behavior of most polymers can be classified as somewhere in between elastic solids and liquids. At low temperatures and high rates of

strain, they act like solids in that they obey Hooke's Law and the stress is proportional to the strain and independent of strain rate. However, at high temperatures and low strain rates, they exhibit viscous properties and follow Newton's Law where the stress is proportional to the strain rate and independent of strain. These behavior trends are the reason that polymers are characterized as viscoelastic materials (9:2-3;15:322).

Rheological Models

Rheological models are used to provide a visualization of what is happening in a material under mechanical loading. These models are composed of both springs and dashpots due to the fact that neither element alone can represent polymer behavior well. These elements can be combined in multiple ways to produce different results. Both the spring and dashpot bring unique qualities that allow the models to represent viscoelastic behavior.

Spring elements are included in the models to represent a perfectly elastic solid. When subjected to an instantaneous stress σ_0, the spring element will respond with an instantaneous strain, ε_0, according to the equation:

$$\sigma_e = E\varepsilon_e \qquad (1)$$

where E is the Young's modulus. Note that for a pure Hookean spring all inertial forces can be neglected.

The dashpot element represents a perfectly viscous material, consistent with the behavior that polymers display when subjected to high temperatures and low strain rates. Response of the dashpot element is described by the Newton's Law:

$$\sigma_v = \eta \dot{\varepsilon}_v \qquad (2)$$

where η represents the viscosity of the material. By including the strain rate in the governing equation of the model, the material behavior is made dependent on time as well as stress and strain. Three popular rheological models that are considered include the Maxwell, Kelvin-Voigt, and Standard Linear Solid Models(1:139-140;9:52;15:323-324;23).

Maxwell Model

The Maxwell model was suggested by J.C. Maxwell and includes a spring and dashpot in a series combination. The Maxwell model can be seen in Figure 2.

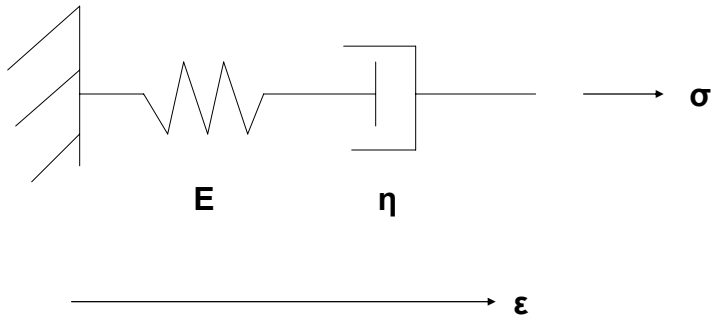

Figure 2. Maxwell Model

Due to the fact that the elements are in series the stress and strain of the model can be represented by the following equations:

$$\text{Total Stress: } \sigma = \sigma_e = \sigma_v \quad (3)$$

$$\text{Total Strain: } \varepsilon = \varepsilon_e + \varepsilon_v \quad (4)$$

$$\text{Total Stain Rate: } \dot{\varepsilon} = \dot{\varepsilon}_e + \dot{\varepsilon}_v \qquad (5)$$

From these equations, the mechanical response to creep and relaxation can be obtained. When in creep, the material is held at a constant stress while in relaxation the strain is kept constant.

The strain response under creep can be derived by considering the total strain rate equation (Eq 5) and using Hooke's (Eq 1) and Newton's law (Eq 2) to give:

$$\dot{\varepsilon} = \frac{\dot{\sigma}}{E} + \frac{\sigma}{\eta} \qquad (6)$$

Since the specimen is subject to creep loading, $\dot{\sigma} = 0$. By integrating with respect to time, the creep strain can be represented by the following equation:

$$\varepsilon(t) = \frac{\sigma_0}{E} + \frac{\sigma_0}{\eta} t \qquad (7)$$

where $\frac{\sigma_0}{E}$ is the initial condition. This model can not predict creep behavior of polymers very well. By examining Eq. 7, it is seen that linear behavior will be predicted, which is not realistic. Creep strain vs. time, as predicted by the Maxwell model, is shown in Figure 3a.

Relaxation response can be obtained in a similar manner. Once again, we start with the total strain rate equation (Eq 5), then employ Hooke's(Eq 1) and Newton's Laws (Eq 2). In this case, $\dot{\varepsilon} = 0$. To simplify integration with respect to time, both sides of the equation are multiplied by η, and an integration factor $e^{\frac{E}{\eta}t}$ is used. As a result, stress response during relaxation is expressed as:

$$\sigma(t) = \sigma_0 e^{-\frac{E}{\eta}t} \qquad (8)$$

where σ_0 is the initial condition (1:141-143;9:53-55;15:324-326;23). Stress as a function of time during relaxation, as predicted by the Maxwell model, is shown in Figure 3b.

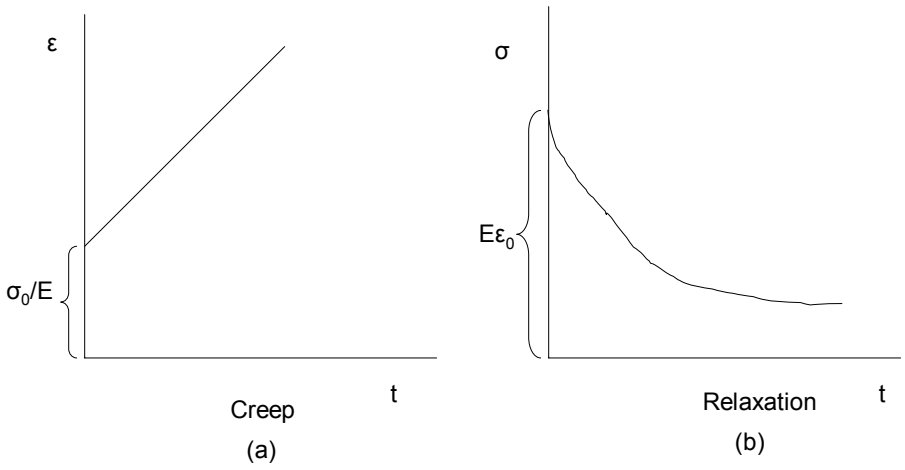

Figure 3. Creep and Relaxation predicted by the Maxwell Model

Kelvin- Voigt Model

The Kelvin-Voigt model is similar to the Maxwell model in that it contains a single spring and a single dashpot. The difference is that the Kelvin-Voigt model has these elements acting in parallel. The Kelvin-Voigt model is schematically shown in Figure 4.

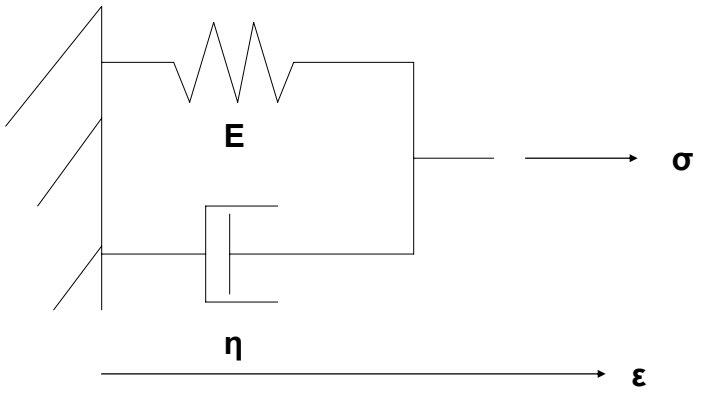

Figure 4. Kelvin- Voigt Model

The parallel action of the spring and dashpot elements in the Kelvin-Voigt model result in different relations between stress and strain of the individual elements, than those obtained for the Maxwell Model. For the Kelvin-Voigt model:

$$\text{Total Stress: } \sigma = \sigma_e + \sigma_v \quad (9)$$

$$\text{Total Strain: } \varepsilon = \varepsilon_e = \varepsilon_v \quad (10)$$

$$\text{Total Strain Rate: } \dot{\varepsilon} = \dot{\varepsilon}_e = \dot{\varepsilon}_v \quad (11)$$

The creep strain can be calculated by starting with the total stress equation (Eq 9). Using the Hooke's (Eq 1) and Newton's Laws (Eq 2), and then dividing both sides of the equation by η, we obtain the following:

$$\dot{\varepsilon} + \frac{E}{\eta}\varepsilon = \frac{\sigma}{\eta} \quad (12)$$

Integration can be carried out using the integration factor of $e^{\frac{E}{\eta}t}$. Using $\varepsilon(0) = -\frac{\sigma_0}{E}$ as an initial condition gives the creep strain response as:

$$\varepsilon(t) = \frac{\sigma_0}{E}[1 - e^{-\frac{E}{\eta}t}] \quad (13)$$

Creep predicted by the Voigt model is shown in Figure 5a.

This model, however, does not predict the relaxation behavior. When the strain rate is set to zero, $\dot{\varepsilon} = 0$, the Kelvin-Voigt model equation (Eq 12) reduces to Hooke's Law. Since strain remains constant, the stress remains constant as well which contradicts the realistic behavior (1:146-148;9:55-57;15:326-327;23). Relaxation behavior predicted by the Kelvin-Voigt model is shown in Figure 5b.

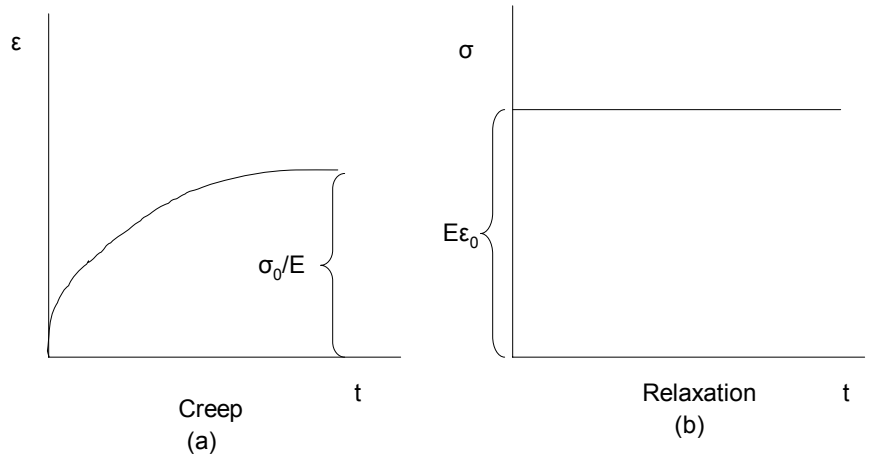

Figure 5. Creep and Relaxation predicted the Voigt Model

Standard Linear Solid

The Standard Linear Solid, schematically shown in Figure 6, is a combination of the Maxwell and Voigt models. It has the advantages of both the Maxwell and Voigt models and none of the pitfalls. Therefore, the standard linear solid can predict both creep and relaxation fairly well.

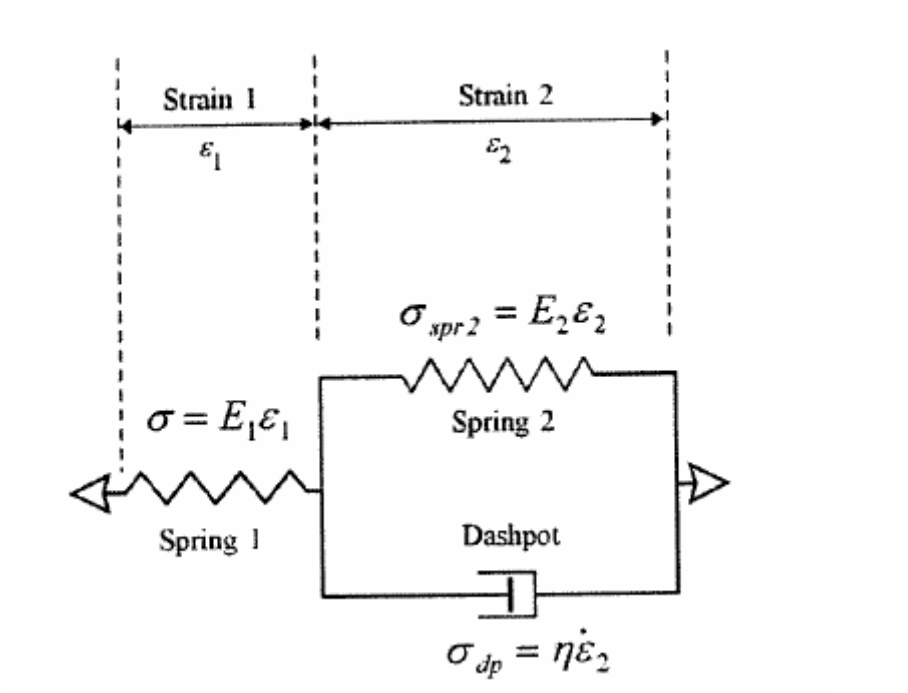

Figure 6. Standard Linear Solid

The equations for this model can be formulated by considering the first spring element as an element unto itself and the parallel combination as the other element. Therefore the governing relationships for each element are:

$$\sigma_{E_1} = E_1\varepsilon_1 \quad (14)$$

$$\sigma_2 = \sigma_{E_2} + \sigma_{\eta_2} \quad (15)$$

$$\sigma_{E_2} = E_2\varepsilon_2 \quad (16)$$

$$\sigma_{\eta_2} = \eta_2\dot{\varepsilon}_2 \quad (17)$$

The relationships for the entire model are:

Total Stress: $\sigma = \sigma_1 = \sigma_2$ (18)

Total Strain: $\varepsilon = \varepsilon_1 + \varepsilon_2$ (19)

Total Strain Rate: $\dot{\varepsilon} = \dot{\varepsilon}_1 + \dot{\varepsilon}_2$ (20)

A solution for the creep behavior of a material can be obtained by considering the total strain rate equation (Eq 20) (21:400-404;23). By making substitutions, appropriate for each individual element, we obtain the following expression:

$$\dot{\varepsilon} + \frac{E_2}{\eta_2}\varepsilon = \frac{\dot{\sigma}}{E_1} + (1 + \frac{E_2}{E_1})\frac{\sigma}{\eta_2} \quad (21)$$

During creep, $\dot{\sigma} = 0$. With the use of an integration factor of $e^{\frac{E_2}{\eta_2}t}$, equation 21 yields:

$$\varepsilon(t) = \sigma(\frac{E_1 + E_2}{E_1 E_2}) + Ce^{-\frac{E_2}{\eta_2}t} \quad (22)$$

By setting time equal to zero, the initial condition is determined to be $C = -\frac{\sigma}{E_2}$, thus giving the final solution of the strain response as:

$$\varepsilon(t) = \sigma(\frac{E_1 + E_2}{E_1 E_2}) - \frac{\sigma}{E_2}e^{-\frac{E_2}{\eta_2}t} \quad (23)$$

As well as predicting both creep and relaxation, all three of these models are capable of predicting response to a change in temperature. It is important since properties of viscoelastic materials depend greatly on temperature. In these models, viscosity is more temperature-sensitive than the spring constants. To account for this sensitivity, viscosity, η, is represented by the following equation:

$$\eta(T) = a_T(T)\eta(T_R) \quad (24)$$

where $a_T(T)$ is a shift factor and T_R is the reference temperature(9:105;23). The shift factor plays a role when plotting the creep compliance of the material. The creep compliance is:

$$J(t) = \frac{\varepsilon(t)}{\sigma_0} \qquad (25)$$

where $\varepsilon(t)$ is the accumulated creep strain and σ_0 is the creep stress. When comparing the creep compliances at different temperatures on a log-log plot, the curves can be superimposed on each other by a horizontal displacement equal to $\log(a_T)$. This means that the responses occurring at two different temperatures are essentially the same, except one occurs in a reduced time. A material that behaves in this manner is called thermorheologically simple (23).

Linear Viscoelastic Theory

Two conditions must be met for a material behavior to be represented by the linear viscoelastic theory. The first requirement is an easy deduction. The material must follow the laws of linearity, i.e. the stress must be proportional to the strain at any given time. If the stress is doubled, the strain is doubled (23).

The second requirement is that the Boltzmann Superposition Principle must apply. This principle states that if a stress, σ_1, is applied at some time, t_1, and a stress, σ_2, is applied at a later time, t_2, then the strain response will be equal to the sum of the strain responses to each of the stresses σ_1 and σ_2 (9:82-82;15:328-331;23). The Boltzmann Superposition principle can be expressed mathematically as follows:

$$\varepsilon[\sigma_1(t-t_1)+\sigma_2(t-t_2)] = \varepsilon[\sigma_1(t-t_1)]+\varepsilon[\sigma_2(t-t_2)] \qquad (26)$$

A graphic representation of the Boltzmann Superposition principle is given in Figure 7.

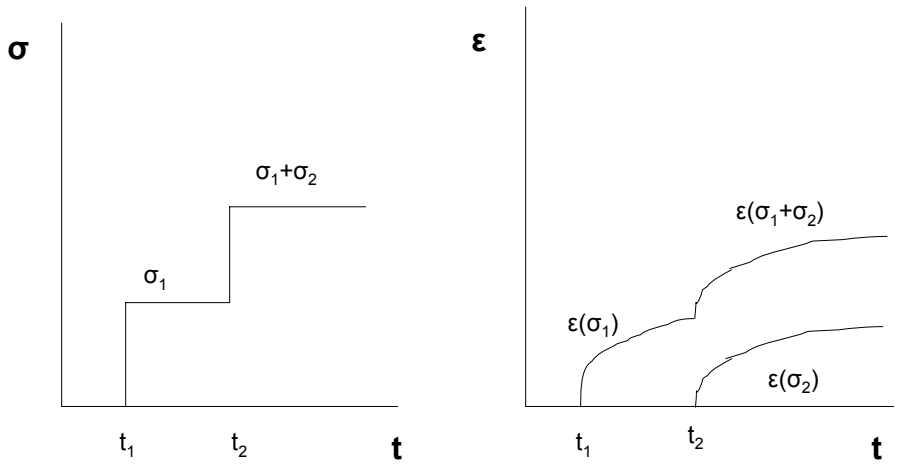

Figure 7. Boltzmann Superposition Principle

Once it is established, that all requirements have been met, the mechanical behavior of the material ought to be examined. Two important areas to look at are the creep and relaxation responses. For creep, the important function was mentioned earlier and is known as the creep compliance (Eq 25). It is important to note that the compliance is only a function of time. In linear theory, this variable will be the only one to appear. As can be seen from the equation, the compliance represents the creep strain per unit of applied stress and it is unique to each material (23;27:219). Because creep is considered a function of the entire loading history, the Boltzmann Superposition principle can be applied to the compliance function. Each loading step makes an independent contribution to creep strain:

$$\varepsilon(t) = \Delta\sigma_1 J(t-\tau_1) + \Delta\sigma_2 J(t-\tau_2) + \ldots \qquad (27)$$

This equation can be changed to account for an infinite number of steps by using an integral:

$$\varepsilon(t) = J_0\sigma_0 + \int_{-\infty}^{t} J(t-\tau)\frac{\partial\sigma(\tau)}{\partial\tau}\partial\tau \qquad (28)$$

where $J_0\sigma_0$ represents the initial compliance (9:84;15:329;23). A similar treatment can be used to determine the relaxation response. The relaxation modulus is defined as:

$$G(t) = \frac{\sigma(t)}{\varepsilon_0} \qquad (29)$$

Then the stress response to multiple loading steps:

$$\sigma(t) = G_0\varepsilon_0 + \int_{-\infty}^{t} G(t-\tau)\frac{\partial\varepsilon(\tau)}{\partial\tau}\partial\tau \qquad (30)$$

Nonlinear Viscoelastic Theory

A material crosses into the nonlinear range when both the compliance and relaxation modulus are no longer functions of time only but also depend on stress or strain (27:219).

$$J(t,\sigma) = \frac{e(t)}{\sigma} \qquad (31)$$

$$G(t,e) = \frac{\sigma(t)}{e} \qquad (32)$$

Furthermore, the Boltzmann Superposition principle does not apply to nonlinear problems. These considerations make solving nonlinear problems much more difficult than accounting for the linear behavior of the material.

A viscoelastic constitutive model capable of predicting mechanical behavior of the material in the nonlinear range was proposed by Schapery (14;24). Schapery's model is

based on thermodynamic principles and is widely used due to the fact that it retains a single time integral form even in the nonlinear range according to Schapery's formulation (18:246). For the case of uniaxial loading, the strain can be represented by the following equation:

$$\varepsilon(t) = g_0 A(0)\sigma + g_1 \int_0^t \Delta A(\psi - \psi') \frac{\partial g_2 \sigma}{\partial \tau} \partial \tau \qquad (33)$$

$$\psi = \int_0^t \frac{\partial \tau'}{a_\sigma} \qquad \psi' = \int_0^\tau \frac{\partial \tau'}{a_\sigma} \qquad (34)$$

In these equations, $A(0)$ and $A(\psi)$ are the initial and transient components of the creep compliance respectively, and ψ is the reduced time function. The constants g_0, g_1, g_2, a_σ are the stress- dependent material functions (18:246).

This model is capable of predicting strain when the stress is applied in a stepwise manner. Take for instance a two- step loading where stress is described as follows:

$$\sigma(t) = \begin{cases} \sigma_a, 0 < t < t_a \\ \sigma_b, t_a < t < t_b \end{cases} \qquad (35)$$

The stress input can be written as:

$$\sigma = \sigma_a [H(t) - H(t - t_a)] + \sigma_b [H(t - t_a) - H(t - t_b)] \qquad (36)$$

where

$$H(t) = \begin{cases} 0, t < 0 \\ 1, t > 0 \end{cases} \qquad (37)$$

Substituting Eq 36 into Eq 33 gives the strain response to the first loading step as:

$$\varepsilon(t) = [g_0^a A(0) + g_1^a g_2^a \Delta A(\frac{t}{a_\sigma^a})]\sigma_a, (0 < t < t_a) \qquad (38)$$

During the second loading step, strain varies with time according to:

$$\varepsilon(t) = g_0^b A(0)\sigma_b + g_1^b[g_2^a \sigma_a \Delta A(\frac{t_a}{a_\sigma^a} + \frac{t-t_a}{a_\sigma^b}) + (g_2^b \sigma_b - g_2^a \sigma_a)\Delta A(\frac{t-t_a}{a_\sigma^b})], (t_a < t < t_b)$$

(39)

In the Eq 38 and Eq 39, the superscripts represent the stress level:

$$g_1^b = g_1(\sigma_b), \text{ etc.}$$

An additional assumption can be made if the material is a polymer resin. Guided by existing experimental evidence for several polymeric resins, one can assume that the time- dependent portion of the creep compliance can be represented by a power law:

$$\Delta A(\psi) = C\psi^n \qquad (40)$$

The case of creep and recovery is represented by equations (41) and (42) when $\sigma_b = 0$. Setting $\sigma_b = 0$ and employing the power law yield the following expressions for creep and recovery strains:

$$\varepsilon_c = [g_0(\sigma)A(0) + Cg_1(\sigma)g_2(\sigma)(\frac{t}{a_\sigma(\sigma)})^n]\sigma \qquad (41)$$

$$\varepsilon_r = \frac{\Delta\varepsilon}{g_1}[(1+\lambda a_\sigma)^n - (\lambda a_\sigma)^n] \qquad (42)$$

where

$$\Delta\varepsilon = \varepsilon(t_1) - \varepsilon(0) = Cg_1 g_2 \psi_1^n \sigma \qquad (43)$$

$$\lambda = (t - t_1)/t_1 \qquad (44)$$

Here $\Delta\varepsilon$ represents the difference between the instantaneous increase and the instantaneous decrease in strain upon application ($t = 0$) and removal ($t = t_1$) of the stress. In the above equations, λ is the non-dimensional time (18:246-248). Use of equations (41) and (42) for various levels of creep stress allows us to obtain material parameters a_σ, g_0, g_1, g_2 as functions of stress, from creep and recovery data.

Previous Work

There are many works in print pertaining to the BMI 5250-4 neat resin, stepwise creep test, or nonlinear viscoelastic modeling.

As for BMI 5250-4, there have been numerous papers written on this subject. For example, it has been included in such works as thermal aging (3), thermal cycling (11), and interlaminar shear strength (7).

The two aspects most relevant to this research are the results from the stepwise creep test and the nonlinear constitutive modeling. Two experimental efforts targeting stepwise creep testing of solid polymers are of particular interest. Krempl and Bordonaro (13) studied the behavior of Nylon 66 under stepwise creep loading. Krempl and Bordonaro also examined how, at a given creep stress level, the creep response during loading differed from that during unloading. Similar investigation was under taken by Westberry (28) for the PMR-15 neat resin at 288 ºC.

The other area of interest was the nonlinear viscoelastic modeling. Nonlinear viscoelastic modeling has been attempted for many different composites. Two well known approaches are those produced by Schapery (14;24) and Pipkins and Rogers (19). All of these following efforts have been based on the Schapery's model in some way.

Among the more helpful papers was that by Perentz and Weitsman (18) that outlined a method for determining the model parameters from stepwise creep and recovery test data for isothermal experiments. Once these parameters were determined, the model was capable of predicting multiple step creep test with a much greater accuracy than the linear theory. This model can also be seen in works done by Elahi and Weitsman (8), Jerina and others (10), and Smith and Weitsman (26). These works calculated the constants in a different manner but included temperature changes.

Thesis Objective

The purpose of this research was to investigate the mechanical behavior of BMI 5250-4 neat resin at 191 ºC. First, the effect of loading rate on basic material properties, such as the Young's modulus was explored. Next the effect of prior loading on creep and recovery response was studied. To accomplish this, the material was subjected to monotonic loading and unloading with intermittent creep tests of a given duration at fixed stress intervals. In addition to both loading and unloading segments, this test also included recovery at zero stress. Finally the nonlinear viscoelastic model (i.e. Schapery's model) was characterized for the BMI 5250-4 neat resin at 191 ºC by means of isothermal uniaxial creep and recovery tests. The model was then validated by means of a multi-step creep test. Reasonable agreement was found between predicted values and corresponding experimental values when the prior stress rates were similar.

III. Material and Specimen

This section will discuss the steps necessary to take the BMI 5250-4 neat resin from uncured resin to the test specimen. Material properties and current applications of the BMI 5250-4 resin are discussed first. Then the fabrication process is outlined. Finally, preparation of test specimens is discussed.

BMI 5250-4 Neat Resin

BMI resins are among the more popular polymer matrix materials on the market today. It offers many unique properties that make it attractive to the aerospace industry. These properties include excellent toughness and a low thermal conductivity. It currently can be found in such components as wing and stabilizer spars, fuselage skins, as well as in the engine components (4).

For testing purposes, this particular material was provided by Cytec Engineered Materials Technical Services located in California. In addition to providing the polymer, Cytec has also made available many of the properties for the BMI 5250-4 resin. In their experiments, they have concluded that this material is capable of performing at temperatures as high as 204 °C but due to its toughness and processibility is more suited for applications in the 82 °C operating temperature range (4). Some important properties of BMI 5250-4 at room temperature with a standard cure are shown in Table 1.

Table 1. BMI 5250-4 Properties

Property	Capability
Tensile Strength	103 MPa
Young's Modulus	4.6 GPa
Strain	4.80%
Coefficient of Thermal Expansion	79.2 x 10^{-6} m/m/ °C
Glass Transition Temperature (T_g)	271 °C

Specimen Fabrication

Resin Processing

The fabrication of neat resin panels is the most important part of the specimen preparation process. If performed poorly, the test specimens will be riddled with defects. These defects can be caused by many events, one being the air trapped in the material.

The raw material was stored in the freezer at the Air Force Research Laboratory (AFRL) Materials and Manufacturing Directorate at Wright Patterson AFB. It was recommended by Cytec that the resin be kept at -18 °C and not be stored for more than six months (4). The frozen resin, milky yellow in color can be seen in Figure 8.

Figure 8. Frozen BMI 5250-4 Resin

The batch of panels, fabricated at AFRL in accordance with the standard procedure, used 350g of the frozen resin. The frozen resin was placed in an aluminum pan, which was then, set in a vacuum oven at 100 ºC for one hour. During this time, the material melted to a liquid state and began to bubble. This step of the process is needed to remove

any moisture that might have been on or in the material in its frozen stage. After one hour in the oven, the liquid material, now dark amber in color, was placed in a conventional oven at 131 ºC for 10 min. During this time the mold was prepared. The mold consists of two sheets of glass clamped together with rubber inserts on the sides to create a seal. The glass plates were coated with mono coat E63 on both sides. This coating ensures that the resin would not adhere to the glass after curing. Once the mold was ready, the liquid resin was poured into the mold using a funnel made from aluminum foil. The funnel was made intentionally small so that the flow of the liquid would not create air bubbles in the mold. This process can be seen in Figure 9.

Figure 9. Transfer of the BMI 5250-4 into the Mold

Next the material was placed in a conventional oven preset to 131 ºC. The material was held at this temperature for 30 min. to allow the bubbles that occurred during the pouring process to exit the material. Air bubbles in the resin can be seen in Figure 10.

After the 30 min. hold, the oven temperature was increased to 191 ºC at a rate of 1ºC/min. The slow rate of temperature increase is necessary for proper curing. The material was held at 191 ºC for 6 h, then post-cured During post-cure, the material was removed from the glass mold and placed in the oven as the temperature was raised to 227 ºC. The material was kept at this temperature for another 6 h. The material processing is now complete.

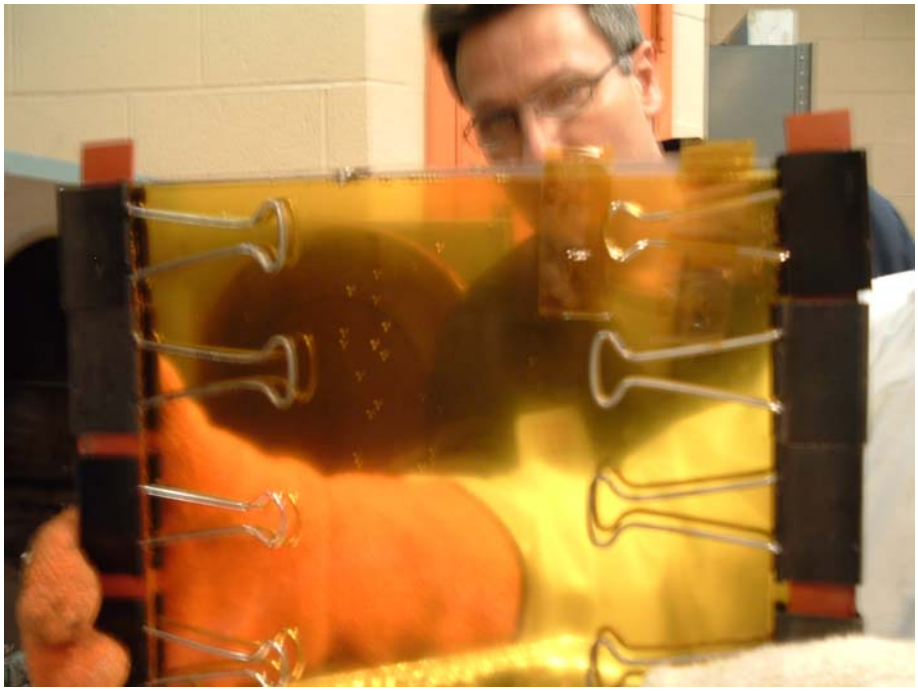

Figure 10. Liquid resin in the mold with visible defects

Test Specimen

Test specimens were machined at the Wright- Patterson machine shop according to specifications in Figure 11 using a water jet process. During this process garnet particles are introduced into high pressure stream of water to cut the material. The actual pressure of the water was 40,000 psi.

Dog-bone shaped specimens with reduced gage section were used to encourage failures in the test section of the specimen. Specimens were not cut from the parts of the polymer panel that showed defects. Likewise, panel edges were discarded.

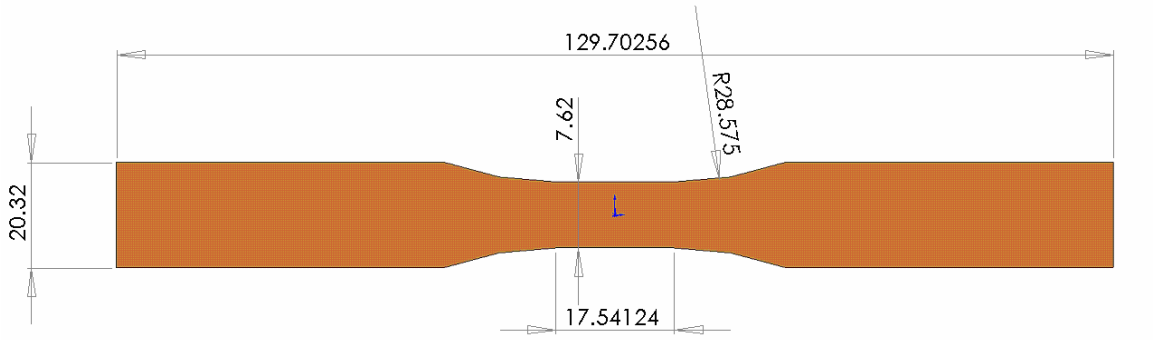

Figure 11. Specimen Geometry. All dimensions are in mm.

Test specimens were tabbed using a glass fabric/epoxy material in order to prevent contact between the specimen and grips. Only the grip portions of the test specimen were tabbed. The tabs had dimensions of 2 cm x 2 cm. The thickness of the tabs was 0.76 mm. The tabs were attached using M- Bond 200 adhesive. A tabbed specimen is shown in Figure 12.

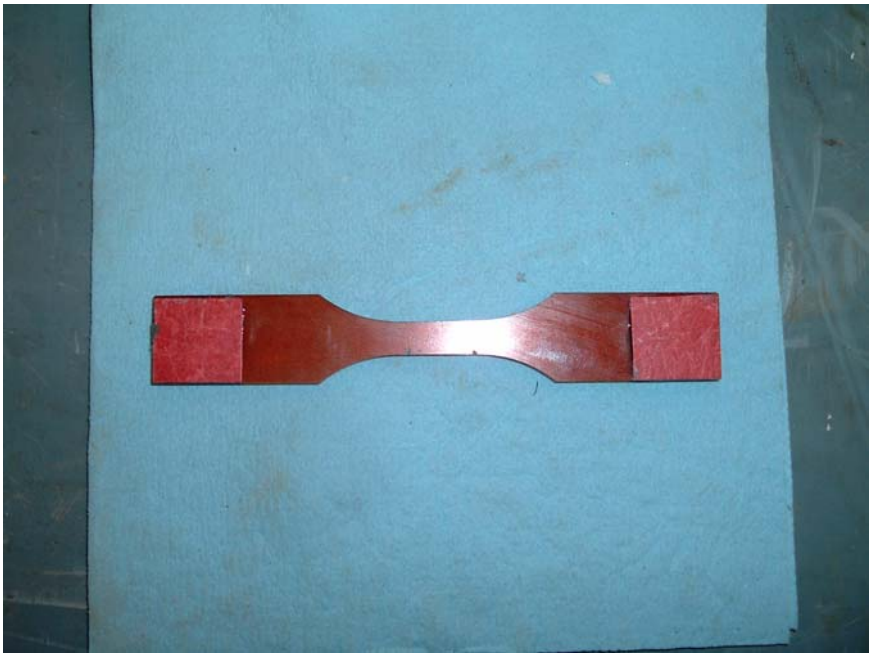

Figure 12: Tabbed Specimen

IV. Experimental Setup and Testing Procedures

Presented in this section is a detailed description of the testing equipment and specific test procedures used in this research.

Experimental Setup

The equipment used in this effort consists of five separate components: the hydraulic machine, the cooling system, extensometer, computer software, and the heating equipment. Every component is critical for proper execution of experiments and accurate data acquisition.

The Hydraulic Machine

An 810 Material Test System (MTS) servo hydraulic machine configured vertically was used in all tests. During the testing of BMI 5250-4 neat resin, the maximum load reached was approximately 1.6 kN (0.35 kips). The load cell fitted with an MTS 609 alignment fixture, had 25.5 kN (5.5 kips) capacity, while the machine capacity was 13.3 kN (3 kips), still more than sufficient to conduct the various tests on BMI 5250-4 neat resin. The testing machine was equipped with MTS 647.02B hydraulic wedge grips that could apply a pressure of up to 21 MPa (3000 psi) to each end of the specimen. Each grip had a pair of flat wedges necessary to grip the flat specimens. The surfaces of the grip wedges were coated with surfalloy to create a gritty surface for better gripping the specimen. Each wedge also had an inlet and outlet to allow cooling water to flow through to keep the wedges and the grips from overheating during high temperature

testing. An anti-rotation device was fitted onto the actuator to ensure that all loading was purely tensile. The overall test setup can be seen in Figure 13.

Figure 13: 3 KIP MTS Hydraulic Machine

The Cooling System

The cooling system was needed for two pieces of equipment: the grips and the extensometer. To function properly the grips must be kept in a -18 ºC to 65 ºC temperature range. Therefore distilled water was kept flowing through the grips. A Neslab chiller was employed to maintain the temperature of the cooling water between 9ºC and 24 ºC. The extensometer was protected from overheating by a heat shield and a cooling air flow.

Extensometer

An MTS model 632.53E-14 extensometer was used for strain measurement. To enable strain measurement in high temperature tests the extensometer is fitted with two 3.5 mm diameter alumina extension rods. Each extension rod had a cone- shaped tip that enabled the extensometer to maintain contact with the specimen that was "dimpled" using an MTS tool designed just for this purpose. The dimples were in the exact shape of the rod tips, and were placed 12.7 mm (0.5 in) apart to correspond to the gage length of the extensometer. Each rod extended 150 mm, which made sure that the extensometer was sufficiently far removed from the heat of the oven. The extensometer was capable of measuring strains in the range of -10% to 20%. It should be noted that electrical noise in the strain measurement cannot be avoided. Such noise may cloud the measurement of very small strains ($\leq 0.005\%$). This consideration should be taken into account when evaluating strain data collected during recovery tests. An extensometer mounted behind the heat shield is shown in Figure 14.

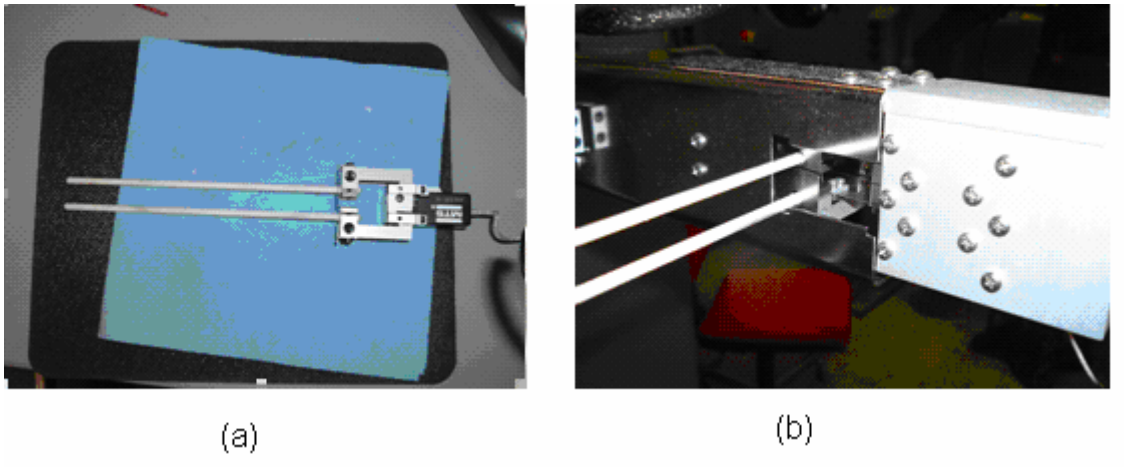

Figure 14: Extensometer Assembly: (a) extensometer and (b) the heat shield

Computer Software

An MTS Teststar II digital controller with associated software was used for both input signal generation and data acquisition. A controller configuration file was created specifically for testing of the BMI specimens. The configuration file contained the set-up information, such as the controller tuning parameters. Next, computerized procedures were developed using the MTS Multi-Purpose Testware (MPT). The procedures communicated the desired test history to both the digital controller and the heating system. In addition, the procedures specified the data acquisition. A view of procedure editor is presented in Figure 15.

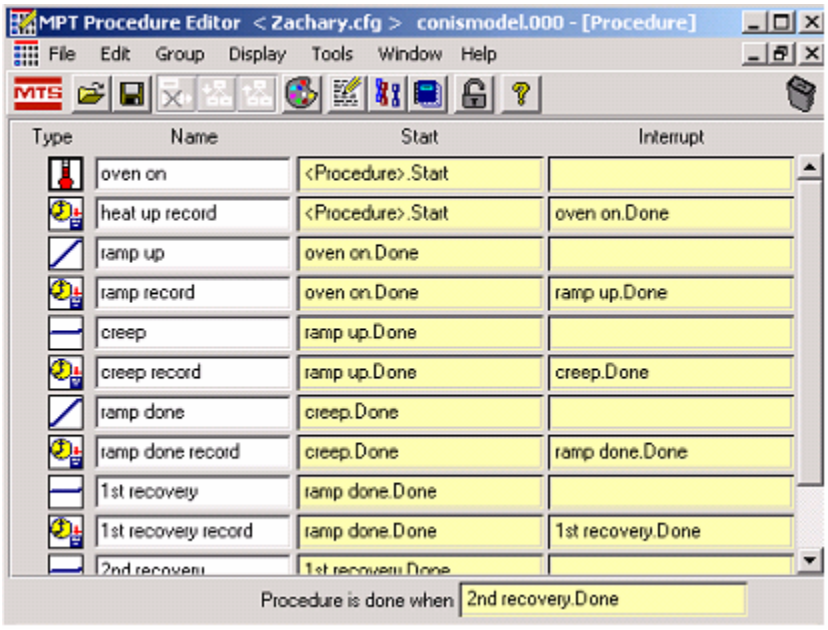

Figure 15: Procedure Editor

The Heating Equipment

An MTS 653 Furnace was used in all elevated temperature tests. The test temperature of 191 °C was on the lower end of the furnace capability which extends to

1400 ºC. The furnace consisted of two halves which would close around the specimen. Each halve was equipped with a silicon carbide heating element and an S- Type non-contact thermocouple. The oven was insulated on all sides with a fibrous alumina insert. Each insert was approximately 18 mm wide. These inserts could be removed and filed down to make slots for both the extensometer rods and the specimen to pass through. During tests, 19-mm section of the specimen would be subjected to the elevated temperature. The temperature was controlled with an MTS 409.83 Temperature Controller, which displayed the left oven temperature, the procedure's desired temperature, and the right oven temperature during the test. A feedback loop between the controller and the right oven thermocouple ensured that the temperature of the oven was close to the procedure's desired temperature. The difference between the temperatures of the two furnace halves was less than 4 ºC. The furnace and the controller are shown in Figure 16.

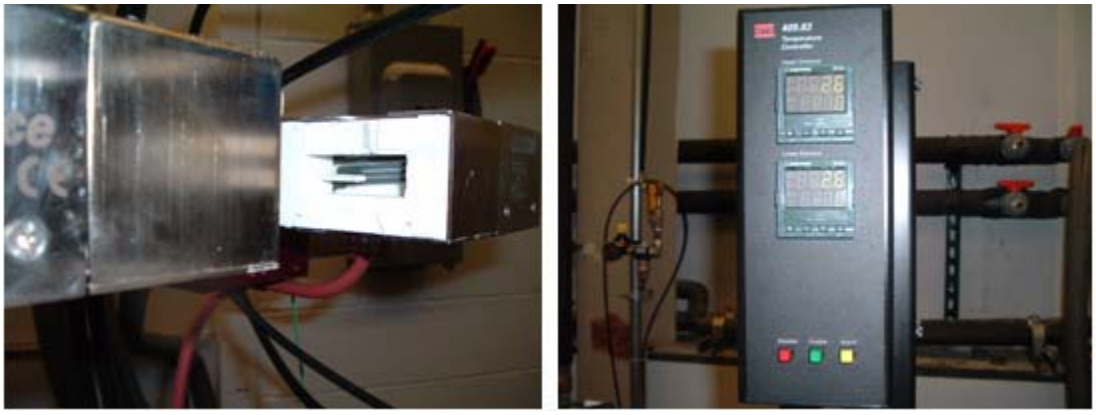

Figure 16: Furnace and Temperature Controller

Experimental Procedures

Prior to starting any experiment, several preparatory steps were completed. First, the chiller was turned on to allow enough time to cool the water that would be circulating

through the grips. Next the machine was warmed up for 30 min. This was accomplished by letting the machine cycle in displacement control. In order to accurately calculate the stress values, the width and thickness of the specimen were measured in three different places in the gage section and the average of each dimension was used to calculate the cross-sectional area. This area was used in stress –load conversions. To ensure that the extensometer maintained good contact with the specimen throughout the test, dimples were put on the specimen edge. With the testing machine in displacement mode, the specimen was locked into the top grip first. The load cell was zeroed out and control was switched to force. Then the bottom part of the specimen was gripped. This method ensured that no load was applied to the specimen before the test began. Then the displacement and strain were zeroed out as well. Finally the extensometer was mounted and oven closed around the specimen. During the heat-up, the machine was kept in force control, in order to allow the specimen to expand freely. Once the test temperature was reached, the specimen was allowed 90 min. to thermally equilibrate. The 90 min. time period was selected as being sufficiently long to allow thermal equilibration, yet not long enough to cause aging of the polymer resin.

Data Collection

In every experiment, force (N), displacement (mm), strain (mm/mm), time (s), Temperature (°C), and command signal were recorded. In displacement controlled tests, the displacement command was recorded. In load controlled tests, force command was recorded. The rate of data sampling varied depending on the test type and the current stage of a particular experiment. Table 2 shows the average rate used in each type of test.

Table 2: Data Collection Rate for specific test segments

Test Type	Time per Point
Heat up/Dwell	1 minute
Monotonic Loading, Stress Rate=1.00 MPa/s	0.5 sec
Monotonic Loading, Stress Rate=0.01 MPa/s	1.0 sec
Creep/Recovery, 1st hr	1.0 sec
Creep/Recovery, >1st hr	5.0 sec

Grip Pressure

A test was necessary to make sure that the proper grip pressure was used. The grip pressure must be high enough to prevent the specimen from slipping while a load is applied, yet low enough to not damage the specimen in gripping. The hydraulic grip manual provides the following formula for calculating the minimum grip pressure for monotonic testing:

$$P = \frac{1.04 \times L}{A} \qquad (45)$$

A = Area of grip piston (cm^2)
L = Max axial load (kN)
P = Grip pressure (MPa)

The area of the grip piston was 16.38 cm^2 and the max load was estimated at 2 kN. With this information, the minimum grip pressure was calculated to be 0.127 MPa. However the grips required pressure of at least 1.03 MPa (150 psi) to close. A tensile test to failure was performed at this grip pressure but the specimen slipped once the stress reached 24 MPa. Therefore the specimen was unloaded and the grip pressure increased to 2.07 MPa (300 psi). Once again, the specimen slipped before reaching failure. The specimen did not fail until a grip pressure of 2.76 MPa (400 psi) was chosen. This grip pressure worked in every test conducted without any slippage or damage to the specimen.

Temperature Calibration

The target test temperature was 191 °C. It was necessary to determine the setting of the temperature controller that would produce the desired temperature on the specimen. The temperature of the specimen was measured by two K-type thermocouples attached directly to the specimen with Kapton tape. The thermocouple wires exited the oven through the holes made for the extensometer rods and were connected to an Omega OMNI-CAL-SA-110 for read-out. Then the oven was heated up to 140 °C at a rate of 1.5°C/min. The slow heat-up rate was used so that the surface of the specimen would not be scorched and damaged. Once the specimen reached 140 °C, the temperature was increased manually while allowing the specimen to dwell after each increase for 5 min. Finally, the temperature controller setting of 160 °C was established that resulted in specimen temperature of 191 ºC. The specimen dwelled at this temperature for 3.5 h to make sure that the specimen's temperature was maintained. The two thermocouple readings fluctuated between 187 °C and 196 °C. The oven temperature fluctuated between 159 °C and 161 °C.

Tuning

Tuning was performed to make sure that the system would respond both smoothly and accurately to commands. Every control mode that was used needed to be tuned. For these experiments, both the displacement and force control were tuned. The displacement control was tuned without using a specimen. However, in order to tune the force control mode, a specimen had to be mounted in the machine. The specimen was subjected to cyclic loading between 10 N and 120 N. By using the oscilloscope, the

feedback force could be compared to the force command. Five settings that could be changed to get a better response: proportional gain (P gain), integral gain (I gain), derivative gain (D gain), feed forward gain (F gain), and forward loop filter (FL filter). Proportional gain was used to increase the effect of the error signal on the servovalve to improve the system response. It played a role in all tuning efforts. The I gain introduced "an integral of the error signal" that gradually boosted the low frequency response of the servovalve command. The D gain introduced a derivative to the feedback signal. It is only important in dynamic tests. The F gain introduced a derivative to the command signal and was responsible for compensation during a phase lag. The forward loop filter adjustments compensated for noise in the servoloop (17:175-180). The best response of the system for BMI 5250-4 neat resin occurred when the values in Table 3 were used.

Table 3: Tuning Parameters

Tuning Parameter	Value
P Gain	7.3
I Gain	0.11
D Gain	0.00
F Gain	0.0028
FL Filter	2048.0 Hz

Monotonic Tensile Test

Three tensile tests to failure were carried out. The first test was performed in displacement control at a rate of 0.025 mm/s. From this test, the load rate corresponding to this displacement rate was calculated. The corresponding stress rate was then calculated as 1.00 MPa/s. To assess effects of stress rate on the properties of BMI 5250-4 neat resin, a stress rate of 0.01 MPa/s was also used. It was important to recognize that these tests may not have reached the ultimate strength of the material, because post-

failure examination of each specimen revealed that fracture had started at one of the dimples. From these tests, two material properties could be determined: the coefficient of thermal expansion and the Young's modulus of elasticity. The elastic modulus was always calculated over the stress range from 5 MPa to 15 MPa. All tests were carried out at 191 ºC.

Creep Test

Two creep tests were carried out at 191 ºC using the load- up stress rates that were employed in the tensile tests. Creep stress was 45 MPa, which corresponds to 80 % of the average maximum tensile stress reached in the tensile test described above. Creep time was 20 h. From this test, the coefficient of thermal expansion and elastic modulus were determined as well as the creep strain and the steady state creep rate.

Recovery Test

This particular type of test was performed four times where two variables were allowed to change. The first two tests consisted of monotonic loading to 45 MPa and unloading to zero stress followed by a 20 h recovery test at zero stress. The magnitudes of stress rates used in these tests were 1.00 and 0.01 MPa/s. The coefficient of thermal expansion and the elastic modulus were determined. In addition the strain variation with time during recovery was assessed. The value of strain measured immediately upon reading zero stress will be referred to as ε_0. The recovery strain is now defined as the difference between the current strain value (measured) and ε_0. Finally, recovery strain as the percentage of ε_0 was evaluated by dividing the recovery strain by ε_0 and multiplied by 100%. The stress-strain behavior in a recovery test is shown schematically in Figure

17. These tests were conducted at 191 ºC and then repeated at 23 ºC. It should be noted that the recovery strain measured at 23 ºC were negligibly small and were within the range of the noise inherent in the system.

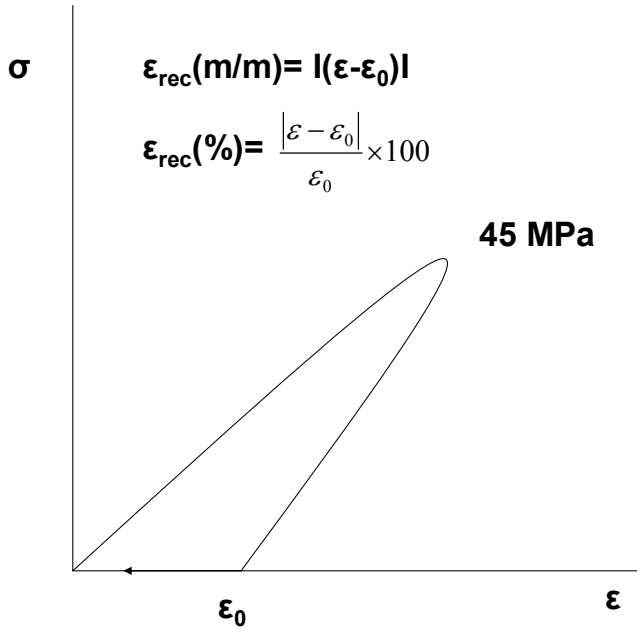

Figure 17: Stress - Strain Curve during a recovery test

Stepwise Creep Test

Stepwise creep test is shown schematically in Figure 18. The purpose of the stepwise creep test was to examine the influence of the prior history on creep and recovery. Two tests were performed at 191 ºC, one at each of the stress rates, 1.00 MPa/s and 0.01 MPa/s. Creep tests of 1 h duration were introduced at 30, 40, and 45 MPa. After unloading to zero stress, a 20 h recovery test was conducted. The results were compared

to those obtained in previous tests to assess the effect of prior history on creep and recovery behavior.

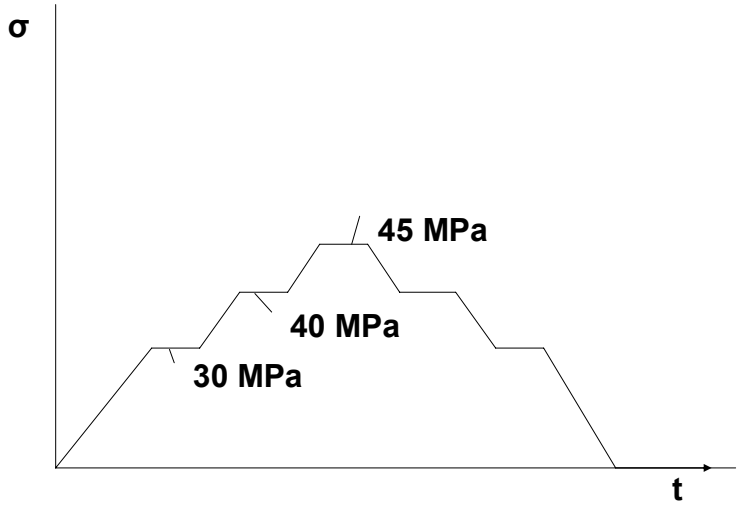

Figure 18: Stress vs. Time Curve during a Stepwise Creep test

Model Characterization Tests

In these tests a specimen was subjected to an instantaneous ramp up to a creep stress level where it would then creep for 30 min. After the creep test, the load was ramped down and recovery at zero stress was recorded. The creep and recovery test is shown schematically shown in Figure 19.

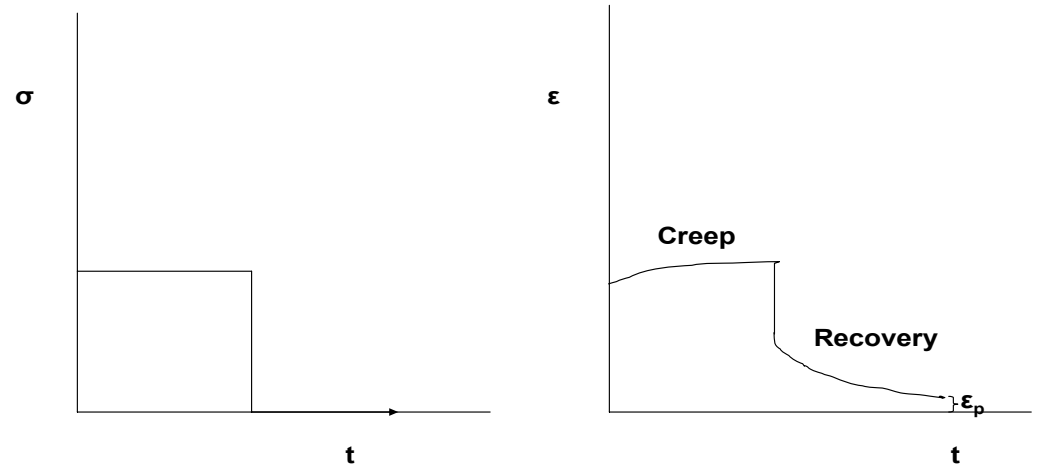

Figure 19: Stress and Strain Response during creep and recovery tests

To characterize the nonlinear viscoelastic model, this test was repeated for various stress levels. The stress levels were fractions of the ultimate tensile strength produced by an undimpled specimen, which was 65 MPa. The creep stress levels and recovery times used in this research are shown in Table 4.

Table 4: Model Testing Stress Levels and Recovery Times

Stress Level (MPa)	% UTS	Recovery Time
8	~12	90
16	~25	300
25	~40	300
32	~50	300
42	~65	300

Note that loading and unloading could not be realized in the step fashion depicted in Figure 19. In reality, loading and unloading were applied at a constant rate of 3 MPa/s

requiring less than 15 s to attain the prescribed stress levels. Every creep and recovery test was triplicated. All creep and recovery tests were conducted at 191 ºC.

V. Results and Discussion

This section summarizes all results obtained in the course of this investigation. First, thermal strains and the calculation of the coefficient of thermal expansion are presented. Next the monotonic stress-strain behavior of BMI 5250-4 neat resin is discussed. Effects of loading rate on deformation behavior and on the elastic modulus are assessed. Then the influence of loading rate and/or loading history on creep and recovery behavior is discussed. Finally characterization and verification of the nonlinear viscoelastic model are presented.

Thermal Expansion

The thermal strain was recorded during every test when the material temperature was raised to 191 ºC. The coefficient of thermal expansion (α) could be calculated using the following relationship:

$$\varepsilon_{th} = \alpha * \Delta T \quad (46)$$

Initial temperature (i.e. room temperature) was approximately 24 ºC. The results can be seen in Table 5. The average value for α was calculated at 64.6 10^{-6}/ºC with a standard deviation of 2.58. This average was slightly lower than the value provided by Cytec. There was not a noticeable difference between the coefficients of thermal expansion calculated for the specimens from panels 1 and 2.

The thermal strain was recorded for each specimen. This value represented the maximum thermal strain the specimen would reach during heat-up to 191 ºC. Note that a slight drop in strain was observed during the dwell period. This drop in strain was

generally less than 0.2% and was due to thermal equilibrium of the specimen. Surprisingly, specimens from panel 2 exhibited a much smaller drop in thermal strain during the dwell period than the specimens from panel 1.

Table 5. Thermal Strain Results

Test	Panel	Thermal Expansion (10^{-6}/ºC)	Thermal Strain (m/m)
Tensile to failure @ 191C	1	62.2	0.0078
Tensile to failure @ 191C	1	61.6	0.0081
Tensile to failure @ 191C	1	60.0	0.0076
Creep	1	66.7	0.0086
Creep	1	65.5	0.0079
Recovery	1	64.0	0.0079
Recovery	1	63.2	0.0079
Step	1	65.4	0.0082
Step	1	62.9	0.0077
model(8 MPa)	1	66.5	0.0084
model2(8 MPa)	2	65.3	0.0087
model3(8 MPa)	2	63.5	0.0086
model (16 MPa)	1	68.8	0.0089
model2(16 MPa)	2	61.6	0.0083
model3(16MPa)	2	68.2	0.0090
model (25 MPa)	1	60.8	0.0081
model2(25 MPa)	2	64.9	0.0087
model3(25 MPa)	2	64.7	0.0088
model (32 MPa)	1	67.0	0.0088
model2(32 MPa)	2	65.6	0.0085
model3(32 MPa)	2	61.6	0.0085
model (38 MPa)	3	61.1	0.0078
model (42 MPa)	1	68.5	0.0092
model2(42 MPa)	1	64.5	0.0083
model3 (42 MPa)	1	68.6	0.0089

Monotonic Tension

Basic tensile properties, namely the elastic modulus and the Ultimate Tensile Strength (UTS), were established in the tensile tests to failure. Furthermore, elastic modulus was calculated based on the results of every test that contained monotonic loading in the

elastic range. However, the UTS could only be evaluated from the results of the three tensile tests to failure. Tensile properties are summarized in Table 6.

Table 6. Tensile Properties at 191 °C

Test	Panel	Rate (MPa/s)	Young's Modulus (GPa)	UTS (MPa)
Tensile to failure @ 191C	1	0.025 mm/s	2.68	55
Tensile to failure @ 191C	1	1	2.77	60
Tensile to failure @ 191C	1	0.01	2.55	54
Creep	1	1	2.53	--
Creep	1	0.01	2.47	--
Recovery	1	1	2.71	--
Recovery	1	0.01	2.53	--
Step	1	1	2.81	--
Step	1	0.01	2.59	--
model(8 MPa)	1	3	2.92	--
model2(8 MPa)	2	3	2.94	--
model3(8 MPa)	2	3	3.12	--
model (16 MPa)	1	3	2.93	--
model2(16 MPa)	2	3	3.15	--
model3(16MPa)	2	3	2.81	--
model (25 MPa)	1	3	3.07	--
model2(25 MPa)	2	3	2.89	--
model3(25 MPa)	2	3	2.99	--
model (32 MPa)	1	3	2.97	--
model2(32 MPa)	2	3	2.94	--
model3(32 MPa)	2	3	3.00	--
model (38 MPa)	3	3	2.93	--
model (42 MPa)	1	3	2.95	--
model2(42 MPa)	1	3	3.05	--
model3 (42 MPa)	1	3	2.97	--

Three tensile tests were carried out at 24 °C. Though performed at different loading rates, they gave an average value of E = 4.4 GPa, which compares well with the modulus value given by Cytec of 4.6 GPa. The average value of the elastic modulus at 191 ºC was 2.85 GPa. It is seen that the modulus dropped by 35 % once the temperature was increased from 24°C to 191 ºC. The room temperature value of the UTS was not

obtained in this effort but the room temperature UTS value given by Cytec is 103 MPa. It must be recognized however, that to obtain accurate strain measurements during these tests, dimples had to be introduced into the specimen surface. There was no test to failure that was conducted without dimples. These dimples acted as crack starters and affected the UTS values measured during these tests. In the first test done, the dimples were not effective in keeping the extensometer in contact with the specimen due to their small size. This test gave UTS of 65 MPa. By this one test, the UTS dropped approximately 37% as the temperature increased from 24 °C to 191 °C This drop in stiffness with increasing temperature was expected due to the fact that in polymers, when the temperature is raised, thermal activation provides increased free volume and motion between the chain molecules. This decrease in stiffness will become more rapid the closer the temperature of the material gets to the T_g (6:35).

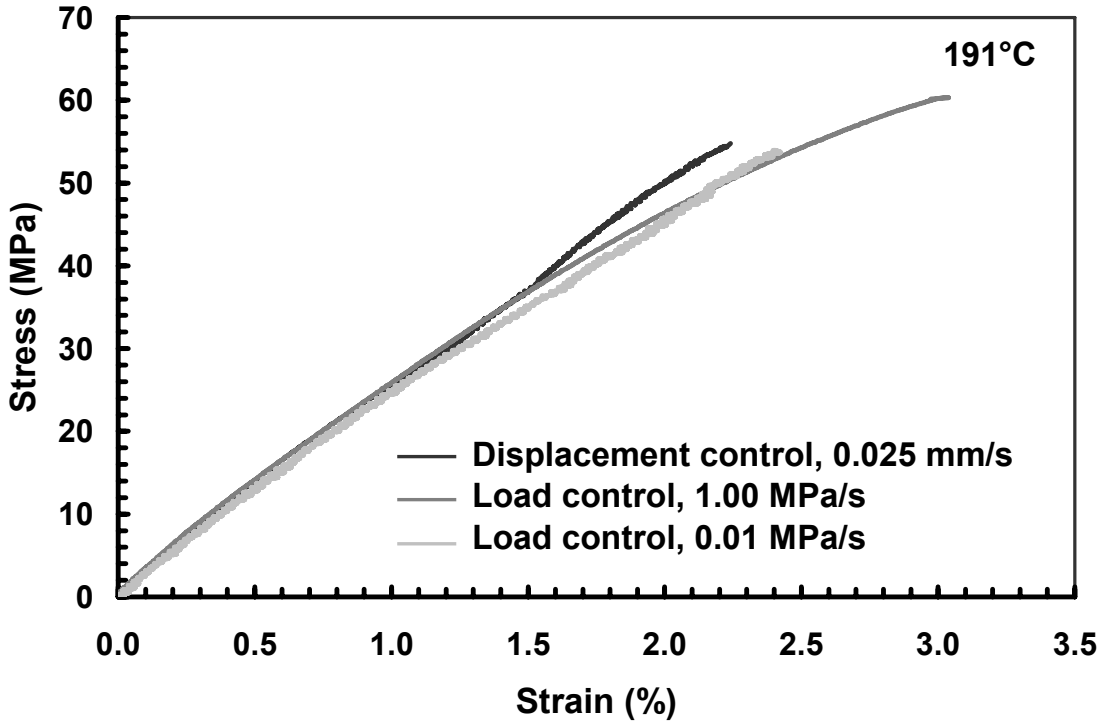

Figure 20. Stress- Strain curves for BMI 5250-4 neat resin at 191 °C

The stress-strain curves obtained for the BMI 5250-4 neat resin are shown in Figure 20. Note that the stress-strain curves do not exhibit a distinct linear range. The slope of the stress-strain curve continues to decrease slowly as the stress is increased. For this reason, the plots were checked and a range was chosen where the stress-strain relation was approximately linear. The Young's modulus was always determined in the stress range of 5 – 15 MPa. It is also seen that fracture occurred when the ultimate stress level was reached. There was no drop in stress before the specimen broke. These results show that the BMI 5250-4 neat resin is brittle at 191 °C. This observation was confirmed when the fractured specimens were examined and no evidence of necking was found.

During these experiments, the effect of stress rate was examined. Three different rates were employed: 0.01 MPa/s, 1.00 MPa/s, and 3.00 MPa/s. It was necessary to have a

difference between rates by at least two orders of magnitude to observe any effect of rate on the Young's modulus. The Young's modulus vs. stress rate is plotted in Figure 21. At first glance, it appears that there is an upward trend, i.e. modulus increases with increasing stress rate. However, several items point to stress rates not having an effect on the Young's modulus. First, the covariance (%) was calculated for all the recorded values of the Young's modulus. The covariance is defined as the standard deviation divided by the average and multiplied by 100. The covariance was 6.91%. Generally, the covariance values below 10% are the result of acceptable data scatter. Furthermore, as seen in Figure 20, the stress-strain curves produced at different stress rates are virtually indistinguishable below 20 MPa. It should also be noted that the majority of the modulus values corresponding to the rate of 3.00 MPa/s were obtained for specimens from panel 2 while modulus values corresponding to the other stress rates were obtained for specimens from panel 1. Thus the slight differences in modulus seen in Figure 21 may be, in fact, due to panel-to- panel variation in the test material. Therefore it was concluded that the stress rate had no effect on the Young's modulus for BMI 5250-4 neat resin for the range tested.

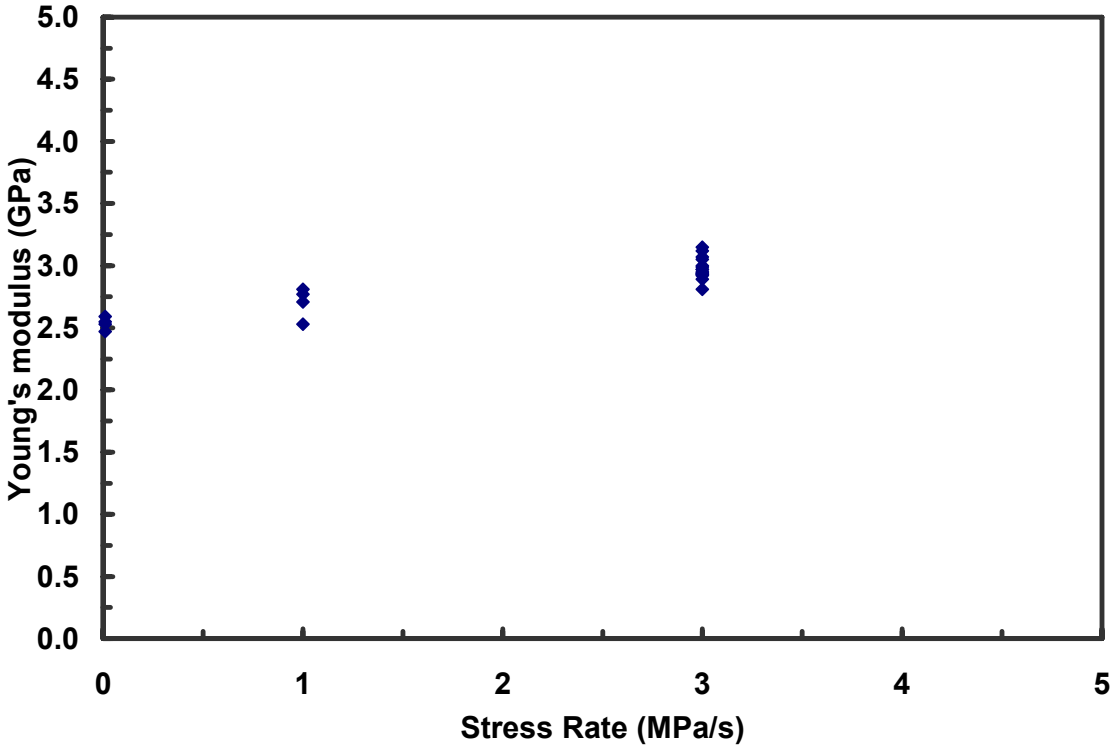

Figure 21. The effect of stress rate on the Young's modulus

Panel-to-panel variability can indeed cause differences in material properties. One small change in the fabrication process can result in a drastic change in material properties. The first panel for this research was made several months before the second and third panels. Furthermore, these panels were made by different individuals, who conceivably varied the processing somewhat. Differences between panels 1, 2, and 3 became apparent in later testing. While specimens from all panels produced similar results at low load levels, specimens from panels 2 and 3 exhibited a significantly different behavior at stresses above 35 MPa than those from panel 1. According to the AFRL technicians, there were numerous reasons that could have caused changes in material strength. The two major quantities that could have been affected by changes in

molding or curing process were the density and the T_g of the panels. Lower values for either of these properties would lead to a lower UTS.

Effect of Prior Stress Rate on Creep Behavior

Two tests were performed to study the creep behavior at different stress rates. The stress rates were 1.00 MPa/s and 0.01 MPa/s. The results of these tests can be seen in Figure 22.

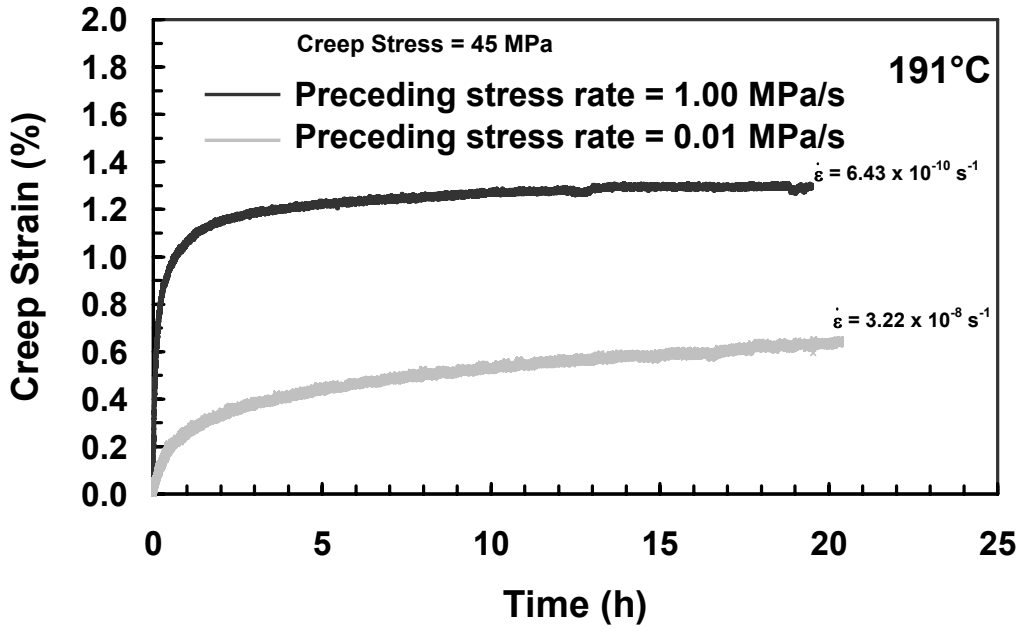

Figure 22. Creep Response due to different stress rates

It can be seen in Figure 22 that the prior stress rate has a considerable influence on the amount of creep strain accumulation. During a creep test, a material can go through three major stages. They are called primary, secondary, and tertiary creep regimes. During primary creep, the strain rate is relatively high but decreases with time. The creep

strain rate is constant during secondary creep regime. This is the minimum creep rate reached in the creep test. This stage can last for a very long time. During the final stage known as tertiary creep, the material is unstable and the strain rate increases quickly until fracture occurs (6:708-709). In the case of the BMI 5250-4 neat resin tested at 191 ºC, the primary creep occurs over the first three hours of the creep test. During this stage, the specimen tested with the higher prior stress rate accumulated approximately three times as much creep strain as the specimen tested with the lower preceding stress rate. This dramatic difference in creep strain accumulations occurs during the first hour of creep. The influence of the preceding stress rate is also seen during secondary creep. The two specimens transition from primary to secondary creep at about the same time. However, they produce very different secondary creep rates. The steady-state creep rate produced by the specimen tested with the lower prior stress rate is two orders of magnitude higher than that produced by the specimen tested with a higher prior stress rate. The secondary creep strain rate was calculated by taking an approximate segment of the creep curve and putting a best-fit linear trend line through it. For these tests, the time segment from 15 h to 18 h was used. These fits can be seen in Figure 23. The material did not transition from secondary to tertiary creep in the given test time. Note that the results obtained here are similar to those obtained by Westberry (28) for PMR-15 neat resin at 288 ºC. Westberry reported that higher creep strains were produced by specimens tested with higher preceding stress rates.

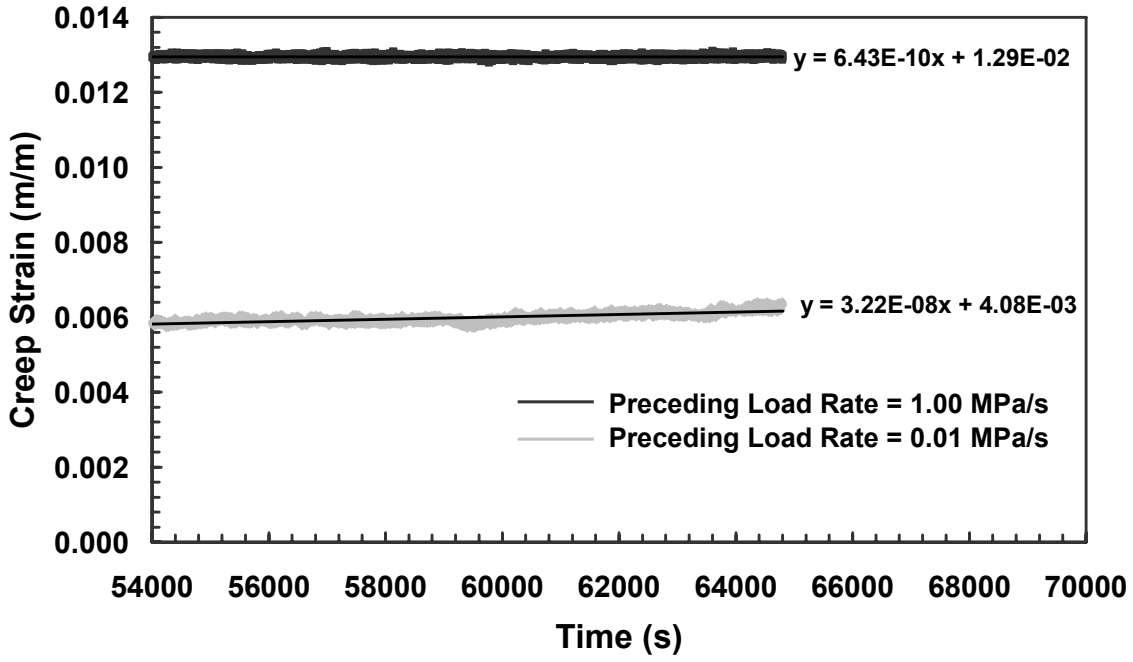

Figure 23. Steady- State Strain Rate

Influence of Prior Stress Rate on Recovery Behavior

The recovery behavior was studied by loading the specimen to 45 MPa, unloading to zero stress, and holding the specimen at zero stress for 20 h. This experiment was repeated twice at 191 ºC using the stress rate magnitudes of 1.00 and 0.01 MPa/s for the loading and unloading segments. In addition these tests were repeated at 24 ºC.

At 191 ºC, the stress- strain curves obtained on the loading and unloading paths were compared. During the load up, the stress-strain curve was linear until the stress reached about 15 MPa. From this point, the slope of the stress-strain curve began to decrease slowly. This decrease continued until the stress of 45 MPa was reached. During unloading, the stress-strain curve remained fairly linear. The modulus between the load and unload parts was compared as well. The modulus was higher during the loading by about 0.2 GPa. This occurred because the load up to 45 MPa took the BMI 5250-4 neat

resin into the plastic region and might have weakened the material. As expected, the material did not return to its original starting strain. The stress-strain curves for both preceding stress rates are shown in Figure 24. At room temperature, the recovery strain was the same magnitude of the noise inherent in the system. Therefore, no conclusions could be made at this temperature.

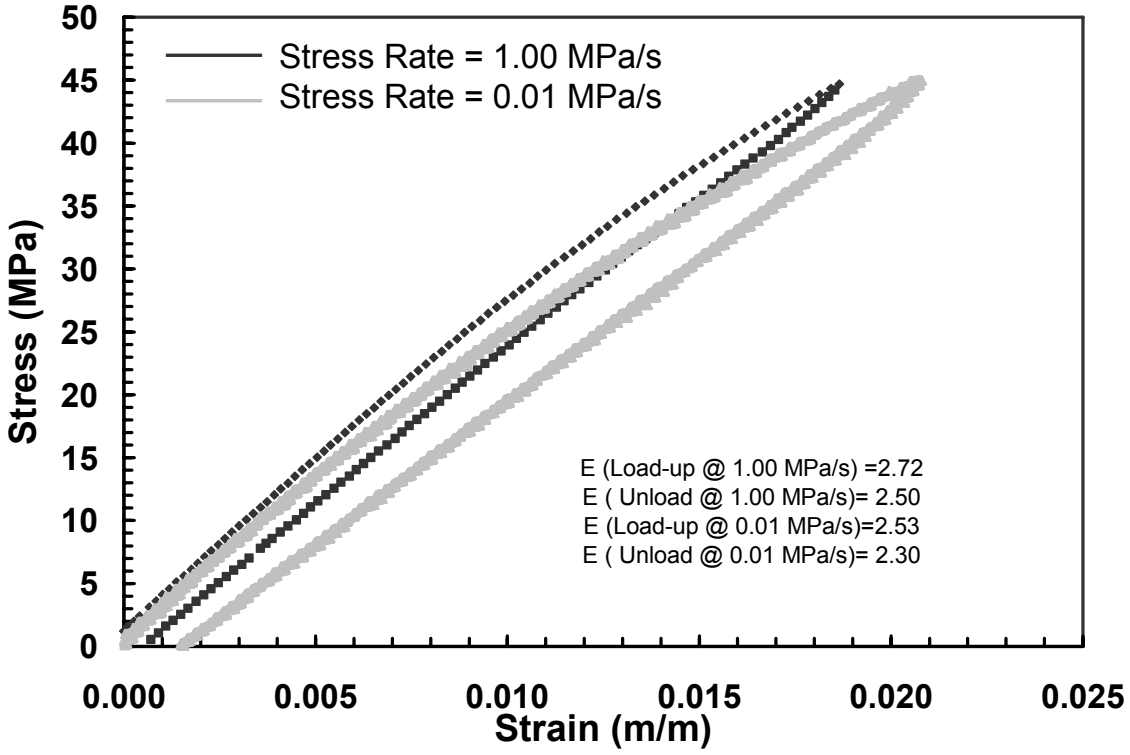

Figure 24. Loading and Unloading of BMI 5250-4 neat resin at 191ºC

The effect of prior stress rate on the recovery behavior was similar to the effect of prior stress rate on creep behavior. The specimens subjected to higher prior stress rate recovered more strain. The results of the recovery tests are shown in Figure 25, where the recovery strain is presented as a percent of the initial strain (i.e. strain recorded immediately after zero stress is reached). It is seen in Figure 25 that the recovery progresses much faster in the case of the specimen subjected to a higher prior stress rate.

It should be noted, however, that because the initial strain were small (<0.001 m/m) so were the recovery strains.

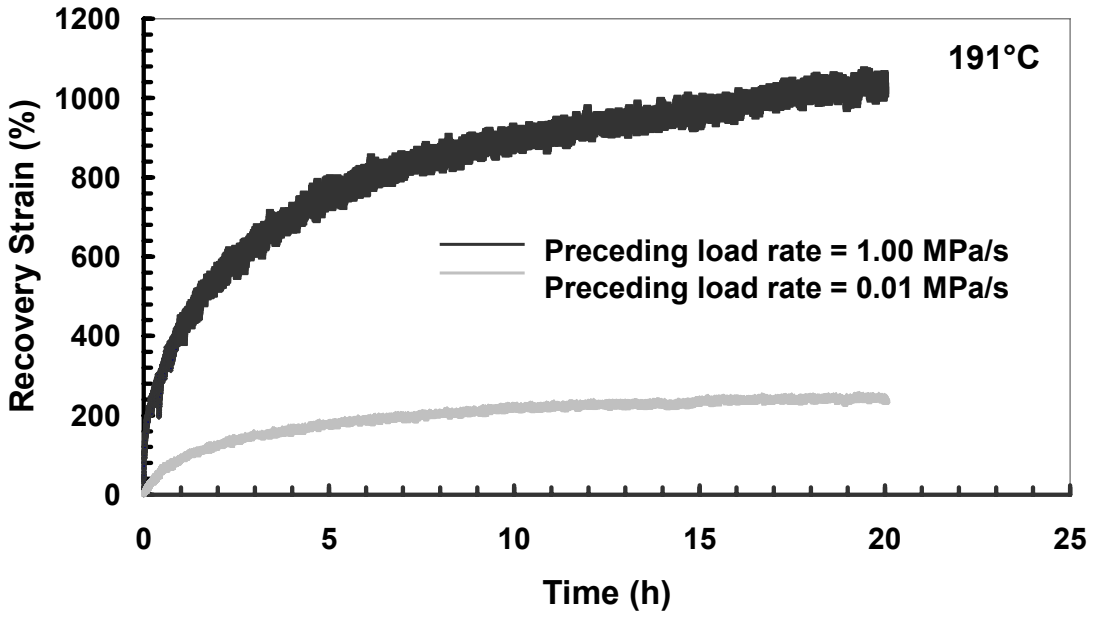

Figure 25. Recovery at zero stress at 191°C. Recovered strain is shown as percentage of the initial value (inelastic strain value measured immediately after reaching zero stress). The effect of prior loading rate on recovered strain is apparent.

Stepwise Creep Test

The purpose of the stepwise creep test was to assess how the BMI 5250-4 was affected by the prior history. During the stepwise creep test the specimen was allowed to creep for 1 h at three different stress levels. The creep stress levels were 30, 40, and 45 MPa. Creep tests were introduced following both loading and the unloading. This test was carried out twice using two different stress rates for comparison.

The first item checked was to see how the stress- strain curve compared to that of the monotonic test (see Figure 26). As expected, the two specimens responded in a similar manner up to the first creep segment. At this point, the stress-strain curve of the stepwise

creep test moves to the right, and continues moving further and further to the right as the test progresses. By the time the 45 MPa creep test ends, the strain accumulated in a stepwise creep test is about 20% greater than that accumulated in a tensile test. An interesting behavior occurs during the creep tests conducted on the unloading path. Instead of increasing strain, the material showed a decrease in strain (i.e. negative creep) during the two creep tests. All of these behaviors were observed at both stress rates.

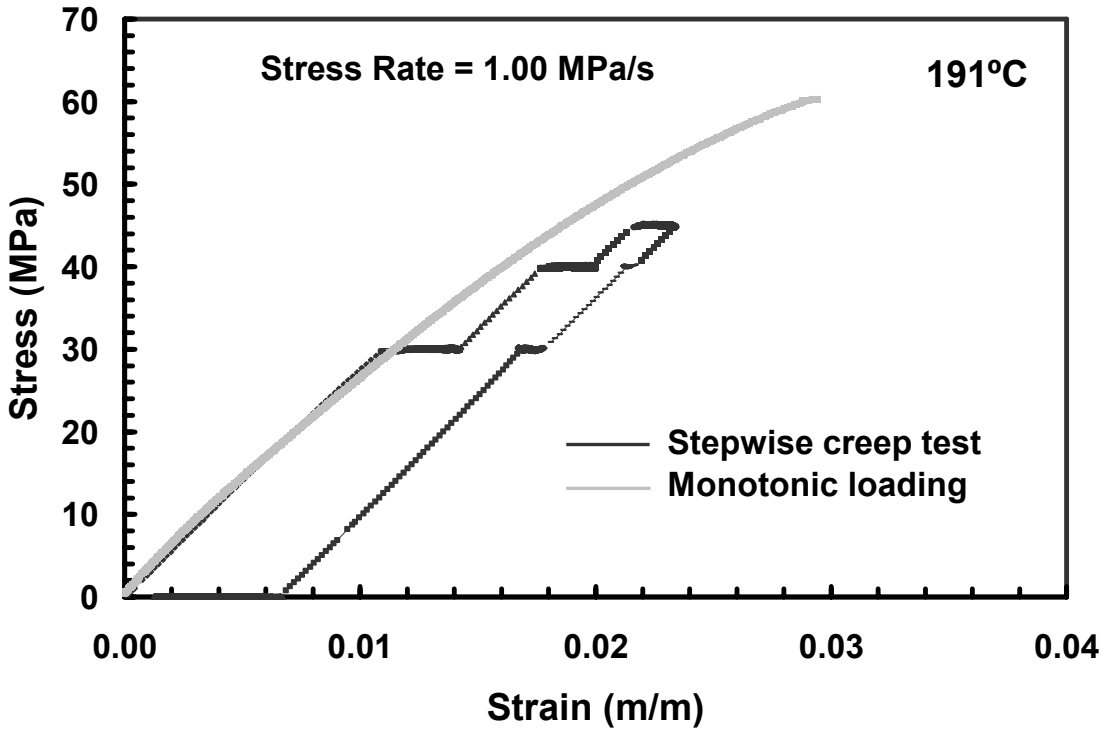

Figure 26. Stress controlled test with intermittent creep periods of 3600 s duration at 191 °C. At the same stress level the creep rate is different during loading and unloading. Negative strain rates are observed in creep tests during unloading. Gray line is an uninterrupted stress-strain curve.

The creep strain was recorded during every creep segment for both stress rates. Results are presented in Figure 27. For each creep stress level, the material exhibited primary creep and appeared to be approaching the secondary creep regime. Two observations are noteworthy. In the test conducted with the 1.00 MPa/s stress rate, the

creep strain accumulation actually decreased with increasing creep stress. This behavior was also reported for PMR-15 (28) for creep stresses in the nonlinear range. Furthermore, the material exhibited negative creep during creep segments on the unloading path. The negative creep strain accumulation increased as the creep stress approached zero. At each creep stress level, the material had a smaller magnitude of negative creep than positive creep it had experienced at that stress level on the loading path. Negative creep has been seen both in polymers such as PMR-15 (28) and Nylon 66 (13) as well as some metallic materials such as steel (22).

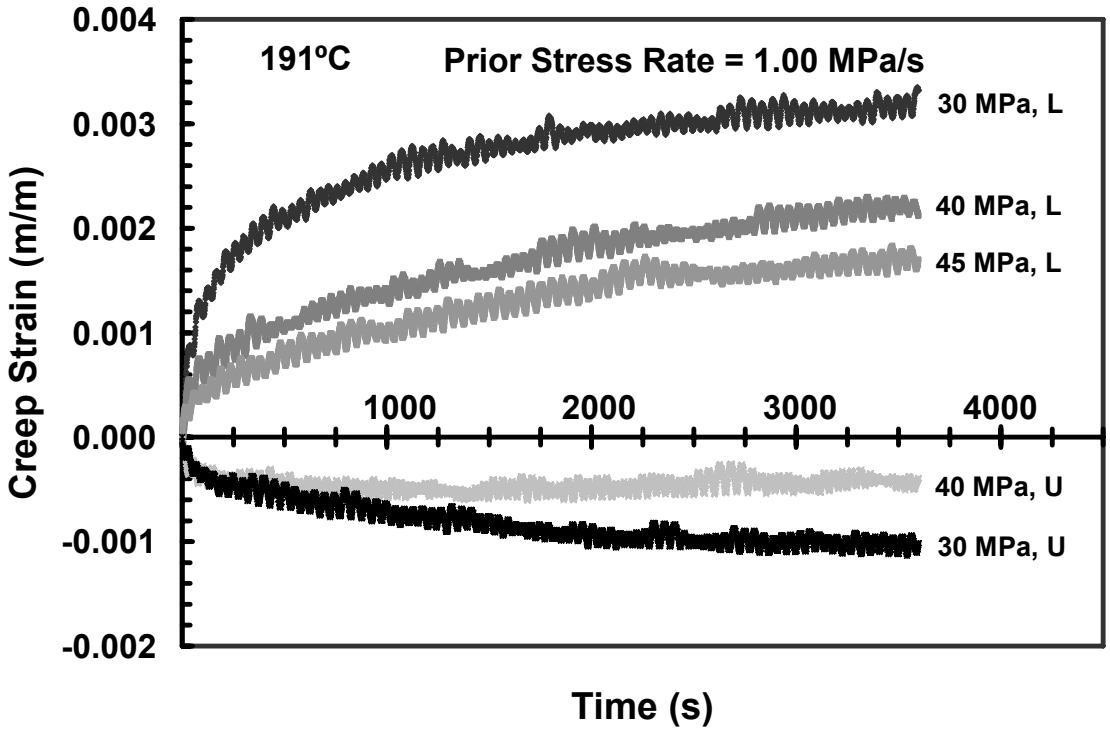

Figure 27. Creep curves pertaining to the stepwise creep test shown in Figure 26. All creep is primary. L = loading; U = unloading.

The specimen subjected to a stepwise creep test with the stress rate of 0.01 MPa/s, exhibited similar creep behavior. Negative creep was observed during unloading

segment, with the negative creep strain accumulation increasing as the creep stress decreased to zero. At a given stress level, the magnitude of the negative creep strain was much less than that of the positive creep strain. As expected, less creep strain was accumulated in a test with the slower stress rate following loading. Another observation is of particular interest. While in the test with higher stress rate, creep strain accumulation (on the loading path) decreased with increasing creep stress, the opposite was noted in the test with the lower stress rate (see Figure 28).

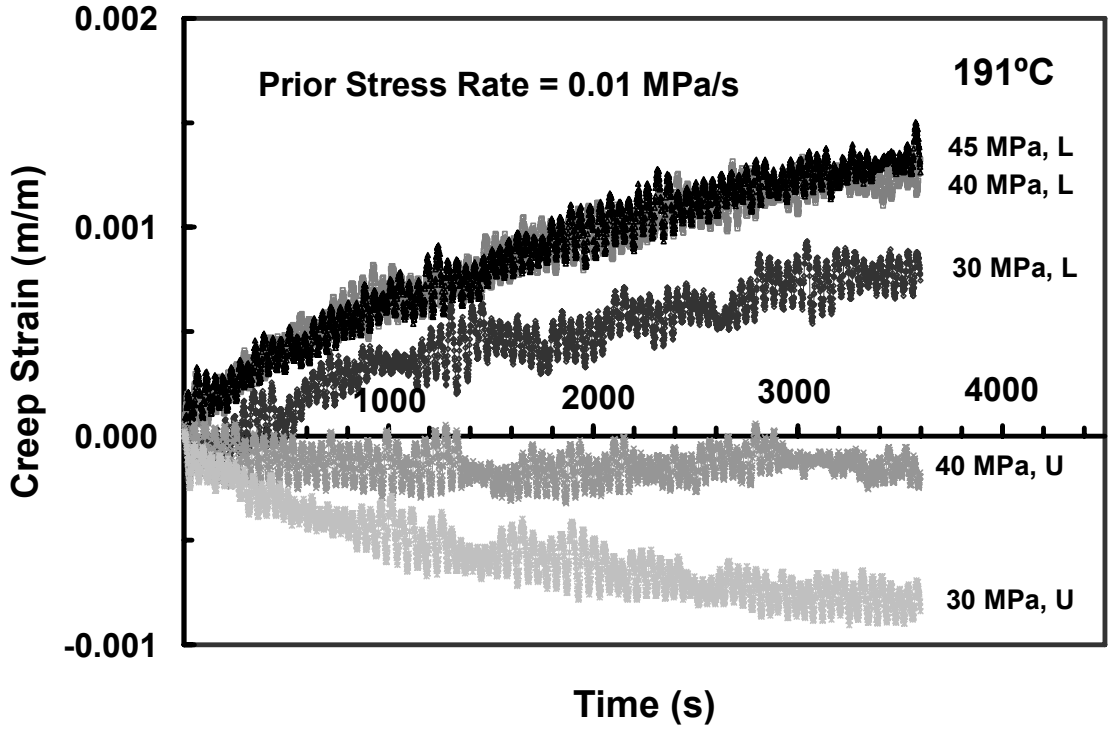

Figure 28. Creep curves pertaining to the stepwise creep test at a prior stress rate of 0.01 MPa/s. All creep is primary. L = loading; U = unloading.

Creep response produced at 45 MPa in a stepwise creep test was compared to that obtained in a creep test preceded by uninterrupted loading at the same stress rate (see Figure 29). Significantly larger strains were accumulated in the creep tests preceded by

uninterrupted loading. For the faster stress rate of 1.00 MPa/s, the strain accumulations differed by approximately a factor of 6, while for the stress rate of 0.01 MPa/s, creep strains differed by nearly a factor of 2.

Similar observations were made regarding the material response during the recovery test at zero stress following the uninterrupted loading/unloading test and the stepwise creep test (see Figure 30). These results show the great effect that prior history can have on a material's mechanical response.

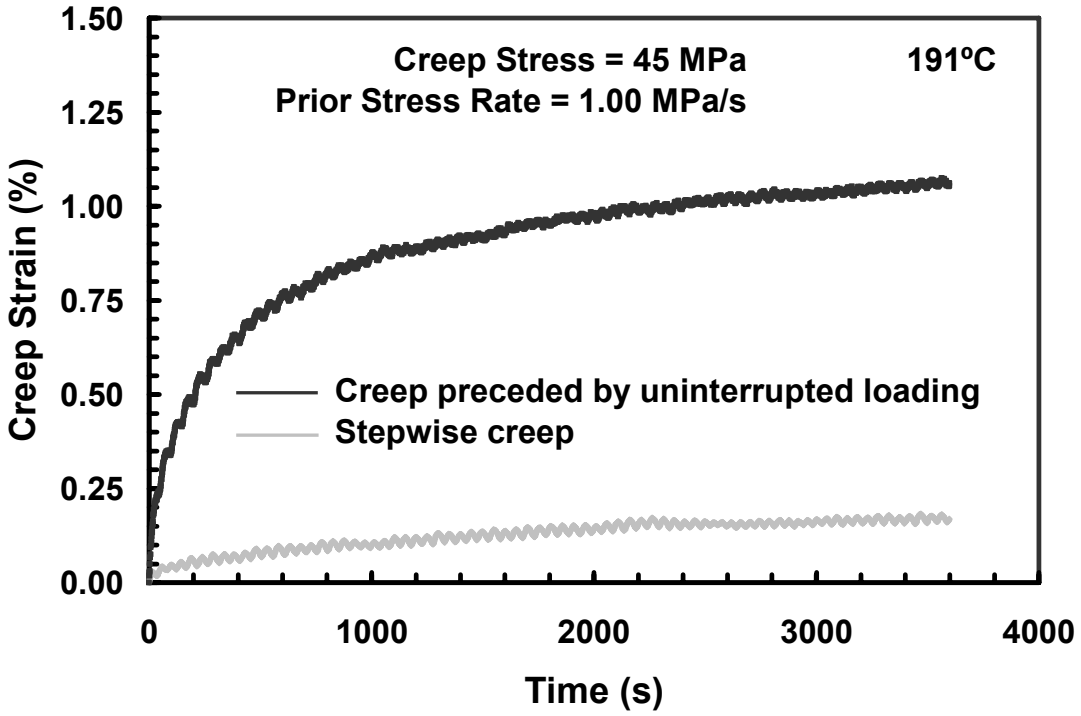

Figure 29. Creep curves obtained at 45 MPa in a stepwise creep test and a creep test preceded by uninterrupted loading. Mechanical strain at the beginning of creep tests are 1.89% (creep preceded by uninterrupted loading) and 2.16% (stepwise creep).

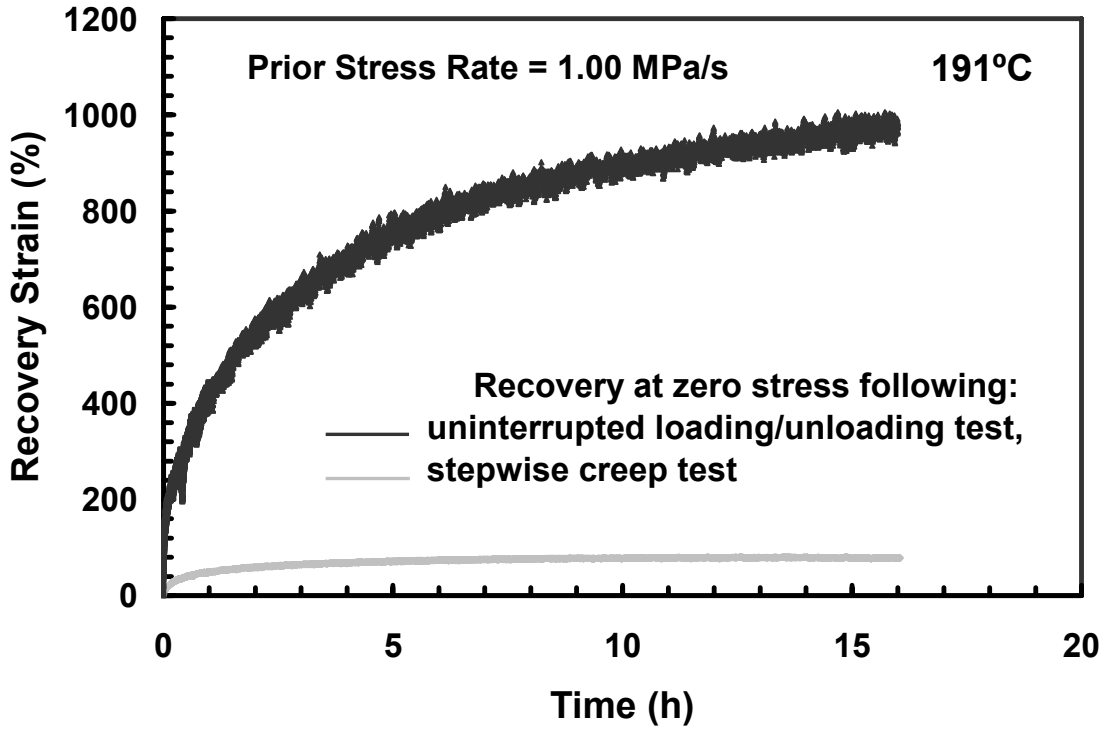

Figure 30. Recovery curves obtained at zero stress in a stepwise creep test and a recovery test preceded by uninterrupted loading/unloading. Recovered strain is shown as percentage of the initial value (inelastic strain value measured immediately after reaching zero stress).

Viscoelastic Model

Data Reduction

The viscoelastic model developed by Schapery (14;24) was characterized for BMI 5250-4 neat resin at 191 ºC. For the case of uniaxial loading, the constitutive equation reduces to:

$$\varepsilon(t) = g_0 A(0)\sigma + g_1 \int_0^t \Delta A(\psi - \psi') \frac{\partial (g_2 \sigma)}{\partial \tau} \partial \tau \qquad (47)$$

The four material constants a_σ, g_0, g_1, g_2 were determined from creep and recovery tests.

Before addressing the constants, it was necessary to determine a threshold stress level, at which the material transitioned from linear to nonlinear behavior. This step was

carried out with the use of isochronous stress-strain curves shown in Figure 31. In the stress-strain curves shown in Figure 31, each point represents the creep strain at a specific time for a given creep stress. The times ranged from 250 s to 1800 s. In the linear range, the isochronous stress-strain curves are linear but as the material moves more and more into the nonlinear range, the isochronous stress-strain curves become nonlinear as well. At 8 MPa, all isochronous curves are right on top of each other. At 16 MPa, the curves are far enough apart to be noticed. This indicates that the threshold stress is between 8 and 16 MPa. After carefully examining the isochronous stress-strain curves, the threshold stress was estimated at 15 MPa.

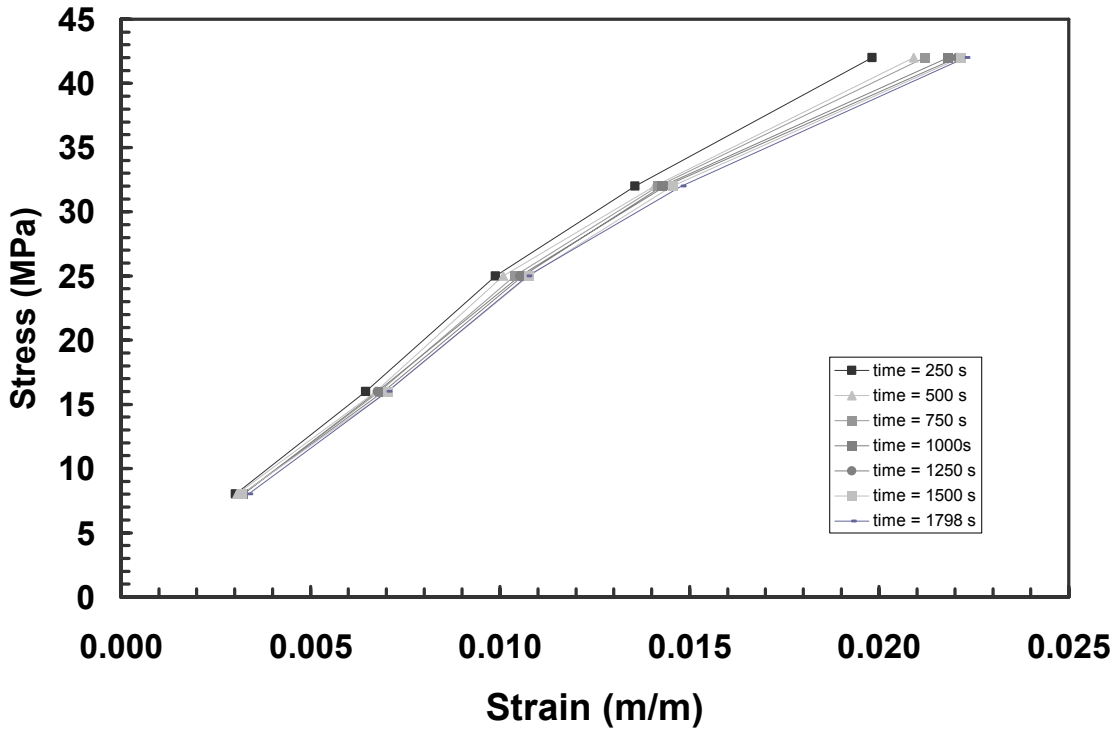

Figure 31. Isochronous stress strain curves for BMI 5250-4 neat resin at 191ºC

During the data reduction, certain steps were followed after every test. First, the ramp to and down from the creep stress was not instantaneous but occurred in less than

15 s. It was necessary to have a fast ramp-up and ramp-down to represent an instantaneous jump. The thermal strain and Young's modulus varied somewhat from specimen to specimen and had to be accounted for. The thermal strain was subtracted from all results, leaving just the mechanical strain. This could be done because all tests were isothermal. It was noticed that specimen-to-specimen variation in modulus could be as much as 0.6 GPa. Therefore to reduce the effects of data scatter, the creep and recovery strains were normalized using the following equation:

$$\varepsilon_{adj} = \frac{E}{E_{avg}}\varepsilon \qquad (48)$$

where $E_{avg} = 2.75$ GPa. In this equation, the actual strain and Young's modulus were divided by the average modulus to get an adjusted strain. This ensured that the effects of data scatter were minimized. In addition, the Young's modulus was measured during every test on both the ramp-up and ramp-down. If the pre-creep and post-creep stiffness values were significantly different, the Schapery model could not be used because it does not account for damage. Finally, the unit for all strains used in the data reduction was microstrain (με).

To begin, it was necessary to develop a reference recovery curve. This curve would be compared to the recovery segments of every single test and be known as the master curve. This master curve was based on the relation between the recovery strain and the reduced time as predicted by Schapery's model:

$$\varepsilon_r = \frac{\Delta\varepsilon}{g_1}[(1+a_\sigma\lambda)^n - (a_\sigma\lambda)^n] \qquad (49)$$

In linear range, it was assumed that $a_\sigma = \frac{\Delta\varepsilon}{g_1} = 1$ which gives

$$[\log \varepsilon_r]_{ref} = \log[(1+\lambda)^n - \lambda^n] \qquad (50)$$

The only unknown in this equation is n. The value of n was determined by using a log-log plot of recovery strain vs. the non-dimensional time, λ, shown in Figure 32. On this plot, several guesses at n were made and resulting curves were compared to the recovery test data obtained at 8 MPa (14;24). Note that the 8 MPa stress level was in the linear range for BMI 5250-4 neat resin. The value of n was determined by comparing the curvatures with the actual recovery strain curve. It is seen in Figure 32 that the prediction made using n = 0.2 best matches the experimental data. However, three tests were conducted at 8 MPa and the average was determined as n = 0.11.

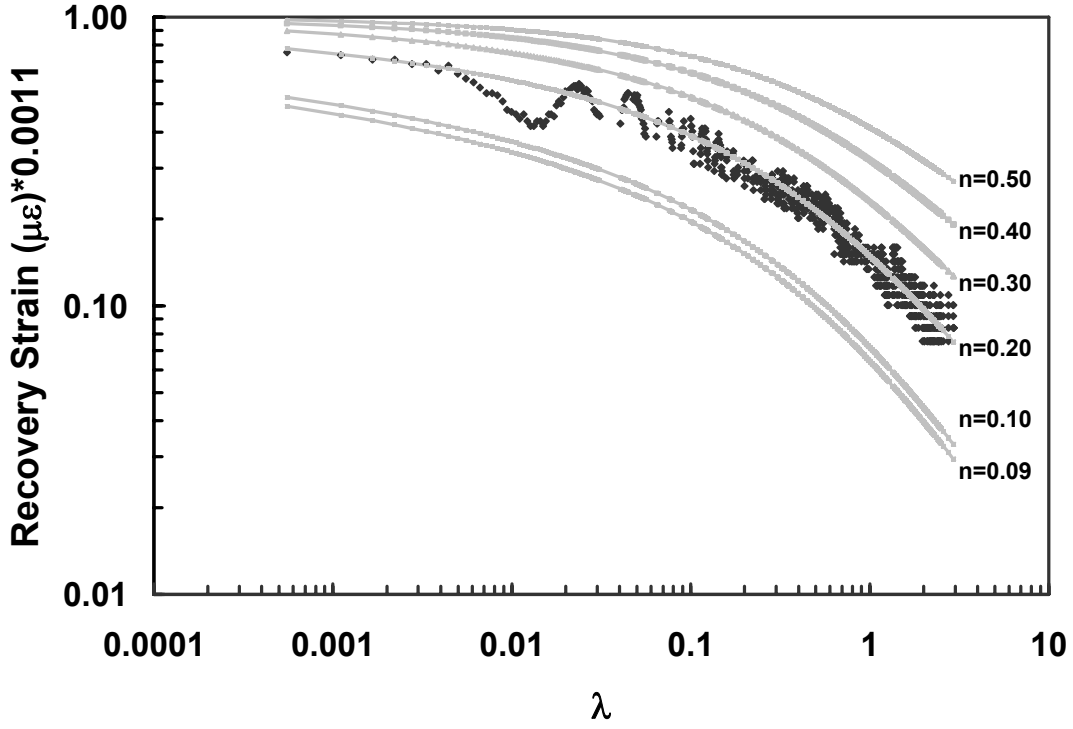

Figure 32. Determination of n. To compare, the recovery strain was shifted downward onto the possible master curves by multiplying by 0.0011

At this point, two more constants could be determined from the material behavior in the linear range. Due to the fact that a_σ, g_0, g_1, g_2 were assumed to be equal to one in the linear range, C and A(0) (see Eq 41) are the only two unknown constants for the 8 MPa test. These values, unlike n, were determined from the creep portion of the test. This calculation was based on the fact that for polymers, the creep behavior can be represented by a power law:

$$\varepsilon(t) = \sigma(D_0 + D_1 t^n) \qquad (51)$$

In the case of the 8 MPa test, $C = D_1$ and $A(0) = D_0$. The constant C was calculated first using the following equation:

$$\varepsilon_{cr}(t_a) - \varepsilon_{cr}(t_b) = C\sigma(t_a^n - t_b^n) \qquad (52)$$

The first time through, C was calculated by taking the average of all the C values when $\varepsilon_{cr}(t_a)$ took on every creep strain value recorded while $t_b = 0$. However, when compared to the actual creep, the fit was slightly off. A better fit was obtained when $t_b = 50s$. The constant A(0), was calculated using a similar equation:

$$\varepsilon_{cr}(t_a) = \sigma(A(0) + Ct_a^n) \qquad (53)$$

Once again, the average value was taken for all the possible A(0) values. The values obtained for all three 8 MPa tests can be seen in Table 7. For these three tests, one specimen came from panel 1 while two came from panel 2. After examining the data, the C and A(0) values obtained from the third test were excluded from further calculations as outliers.

Table 7. 8 MPa Constant Values

Stress (MPa)	C	A(0)	n
8	61.13718	294.0556	0.05
8	59.88323	284.2517	0.1
8	99.75079	217.1469	0.2

With n, C, and A(0) in place, it was now possible to determine the remaining material constants. It was possible to obtain values for both g_1 and a_σ by shifting the master curve on a log- log plot to coincide with the recovery curve for a particular stress level (14;24). It can be seen from Eq 49 that a vertical shift would correspond to $\frac{\Delta\varepsilon}{g_1}$ and a horizontal shift to a_σ. An upward shift of the master curve corresponds to $\frac{\Delta\varepsilon}{g_1} > 1$, while a shift to the right corresponds to $a_\sigma < 1$. To obtain these values, the vertical difference at each point in time between the recovery strain and the master curve was calculated and the

master curve was shifted up by the average value. Then, the curve was moved horizontally to obtain a value for a_σ. Obtained by this method, the value of a_σ was not unique, but could have varied by 0.05 in either direction. Judgment had to be used to select the value of a_σ. The goal of the shift was to have as many points represented on the master curve as possible. Based on these considerations, values of a_σ for every stress level were determined and a trend line was plotted through these points (see Figure 33). The trend line was used only for stress values in the nonlinear range because in the linear range all of the constants are assumed to be 1.

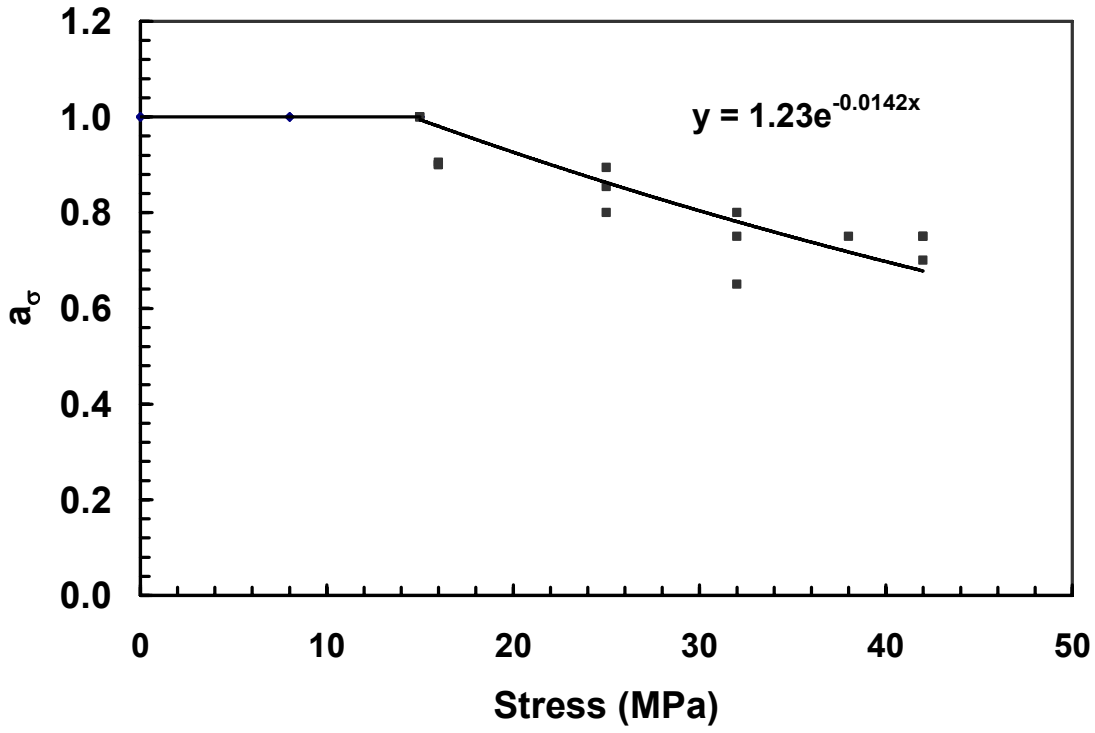

Figure 33. Material constant a_σ as a function of applied stress

The values of g_1 were calculated using vertical shifting of the master curve onto the recovery curve. The value of $\frac{\Delta\varepsilon}{g_1}$ was obtained from the vertical shift. It was possible to calculate $\Delta\varepsilon$ from the creep curve using the following relationship:

$$\Delta\varepsilon = \varepsilon(t_1^-) - \varepsilon(0^+) \qquad (54)$$

This relationship represents the creep strain that was accumulated throughout the entire creep stage (14;24). Once $\Delta\varepsilon$ was established, g_1 was the only unknown and could be solved for. Material constant, g_1, as a function of applied stress is shown in Figure 34.

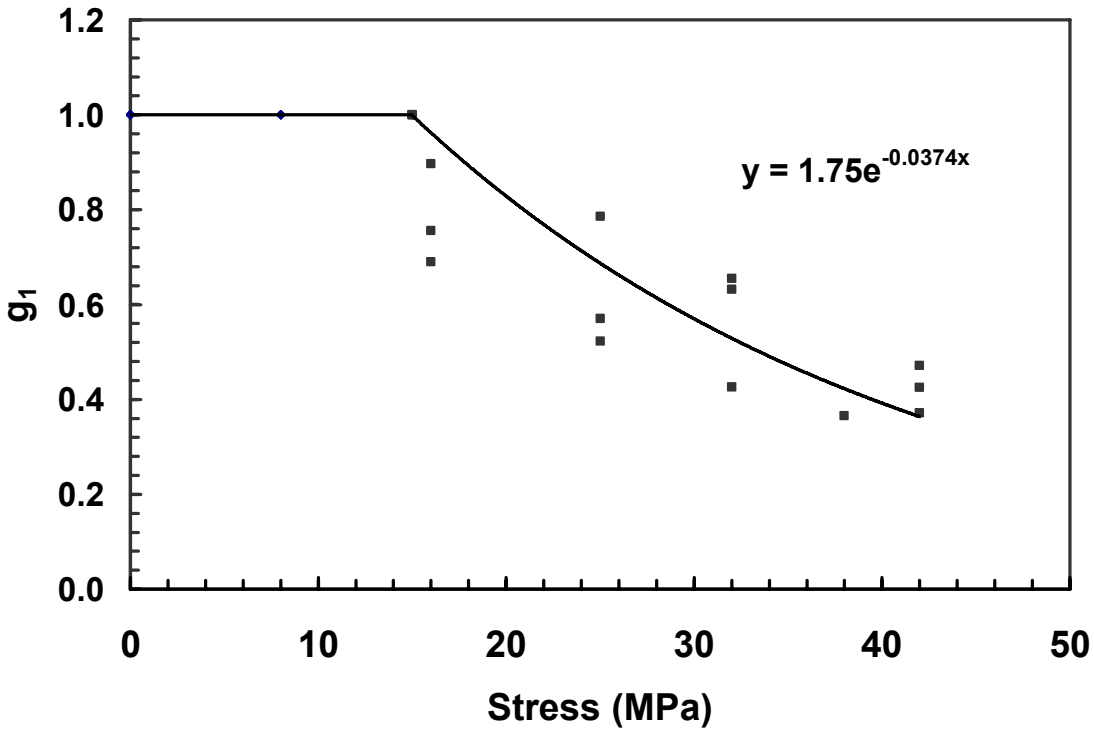

Figure 34. Material constant g_1 as a function of applied stress

The two remaining constants, g_0 and g_2, were calculated using the creep data. By fitting the experimental data with the power law in equation 51, g_0 and g_2 could be found from:

$$D_0 = g_0 A(0) \quad (55)$$

$$D_1 = C \frac{g_1 g_2}{a_\sigma^n} \quad (56)$$

In both equations, the desired constant was the only unknown and could be solved for. Material constants, g_0 and g_2, as a function of stress can be seen in Figures 35 and 36, respectively.

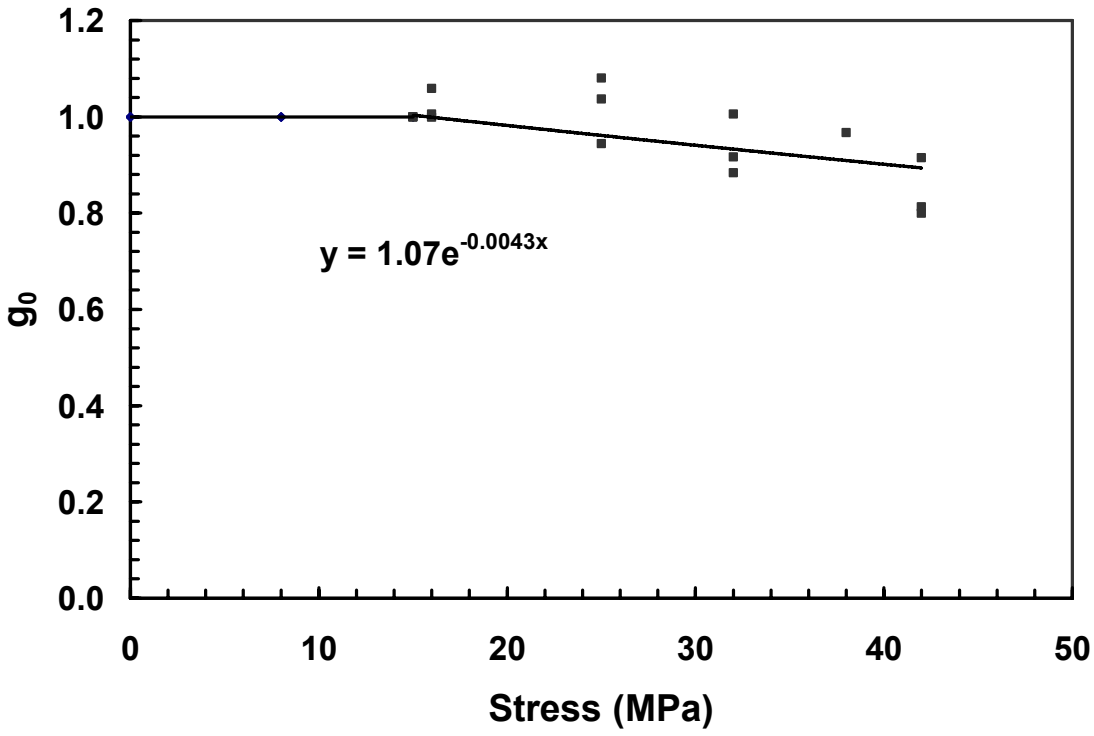

Figure 35. Material constant g_0 as a function of applied stress

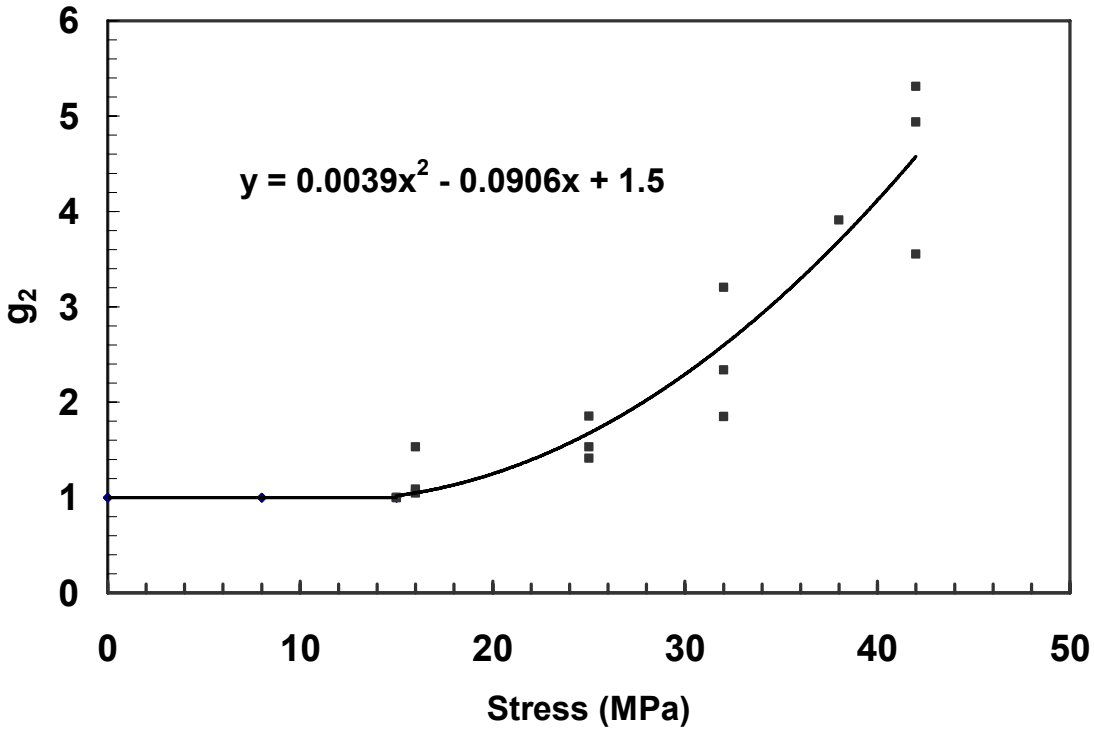

Figure 36. Material constant g_2 as a function of applied stress

Model Verification

Three different kinds of tests were used for model verification. They were a single step creep test with two different prior stress rates, and a stepwise creep test. None of these tests were used to determine the constants for the model.

First the model prediction was compared to the results of a creep test at 45 MPa with the load-up rate of 1.00 MPa/s. This stress rate was of the same order of magnitude as that used in the creep and recovery tests for model characterization. The constants for the nonlinear prediction were calculated using the best fit curves, while for the linear prediction all constants were equal to 1. The results can be seen in Figure 37.

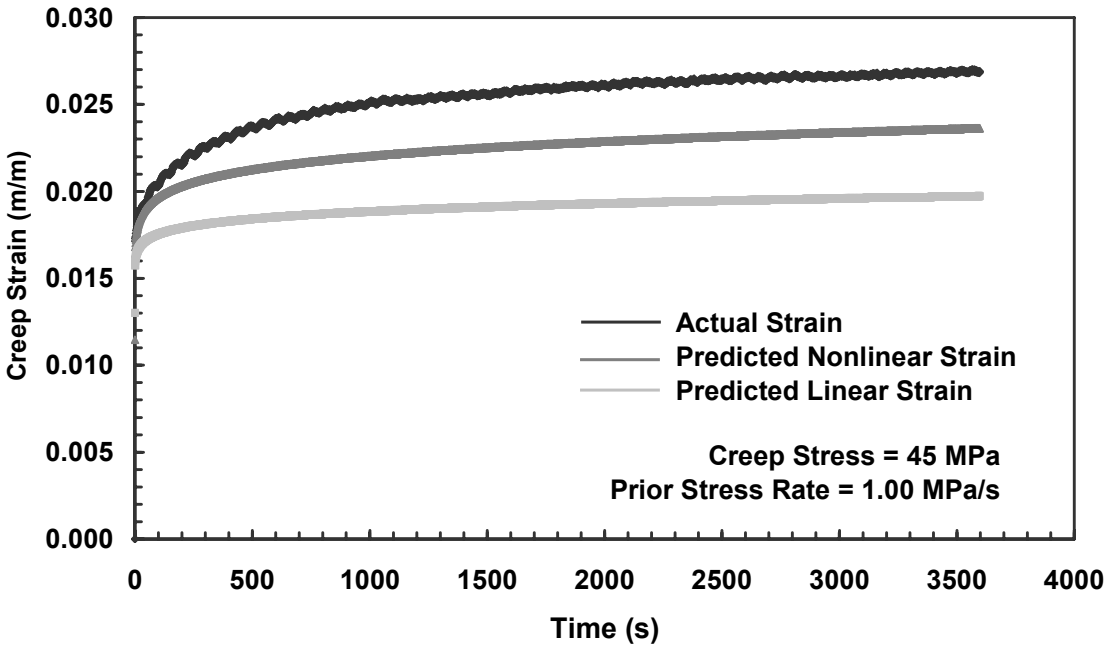

Figure 37. Viscoelastic model predictions of the creep test at 45 MPa

At this stress level, the nonlinear model did not perform well. This may be due to the fact that this stress level falls outside the range of stress values that were used to get the model constants. Another example of the model prediction can be seen in Figure 38. This graph showed that the model was capable of predicting creep well when the creep stress was less than 42 MPa, the highest stress used in the model characterization tests.

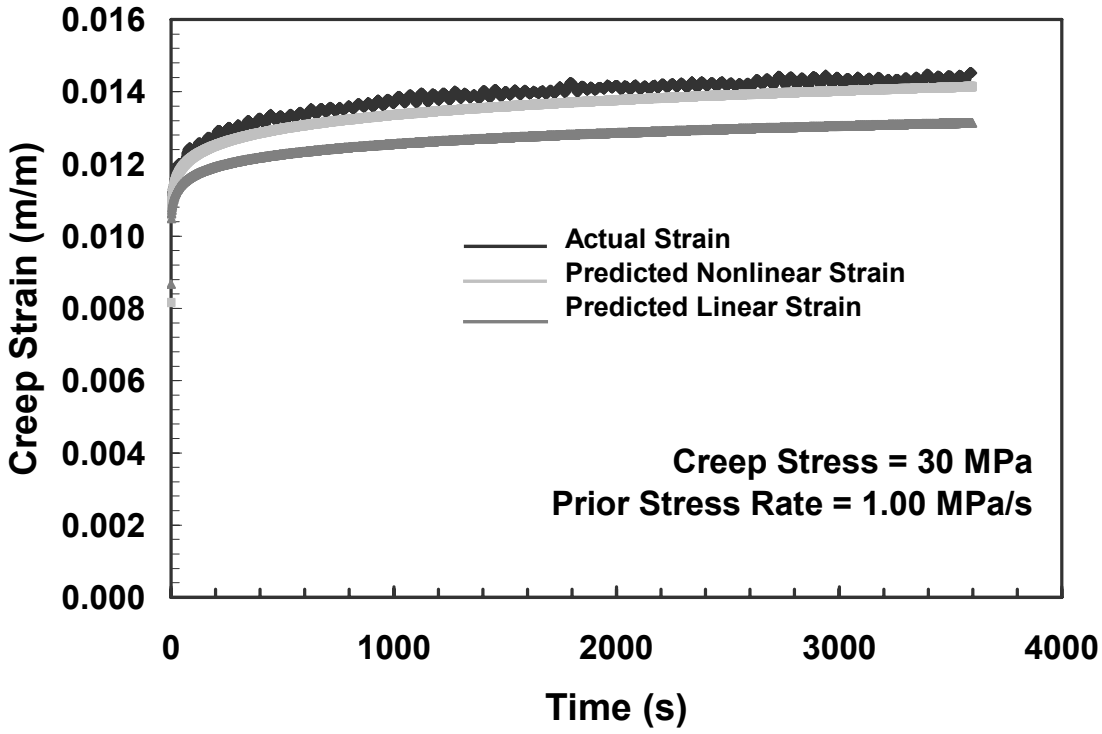

Figure 38. Viscoelastic model predictions of the creep test at 30 MPa

The next test was to see how well the model would predict the results of a creep test with a much slower prior stress rate of 0.01 MPa/s. The prediction for this case can be seen in Figure 39. The viscoelastic model was not capable of accurately predicting the creep response because there was no way to account for the prior stress rate. The only reason for the better results at the faster prior stress rate is that in this case the prior stress rate was fast enough to approach the "instantaneous" load-up used in model characterization. As expected, the linear model was not capable of predicting the creep strain behavior because (a) the creep stress was in the nonlinear range and (b) the model could not account for the prior stress rate.

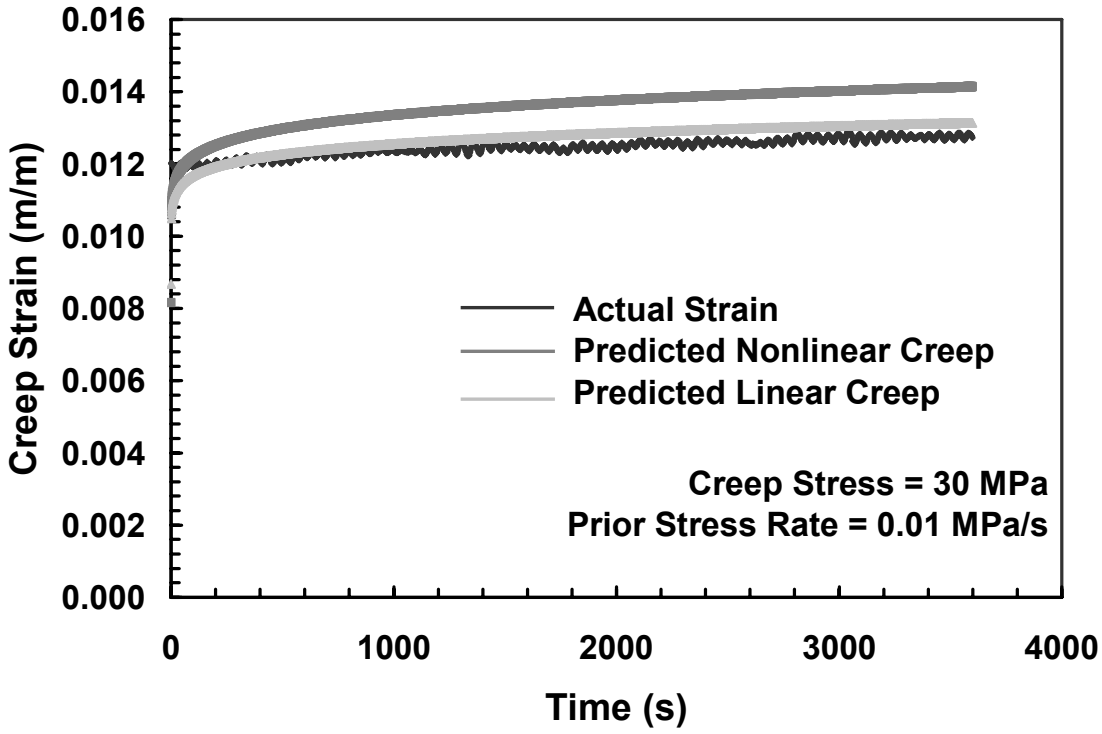

Figure 39. Viscoelastic model predictions of the creep test at 30 MPa

The next test was to see how well the model could predict results of a stepwise creep test. Model predictions were only compared to the test using 1.00 MPa/s stress rate since it has already been demonstrated that the model could not account for the slower prior stress rate. The necessary equation was based on the Schapery's model for the uniaxial loading:

$$\varepsilon(t) = g_0 A(0)\sigma + g_1 \int_0^t \Delta A(\psi - \psi') \frac{\partial g_2 \sigma}{\partial \tau} \partial \tau \qquad (57)$$

In the case of multiple loading steps, applied stress as a function of time can be expressed as follows:

$$\sigma(t) = \sigma_a [H(t) - H(t - t_a)] + \sigma_b [H(t - t_a) - H(t - t_b)] + \ldots \qquad (58)$$

This stress function would account for every step that the specimen would experience during a stepwise creep test. Therefore, for the case of the stepwise creep test performed here, six stress levels had to be accounted for to describe the entire test, including recovery at zero stress. As expected the equation became progressively more complicated as more steps were included. The model predictions can be seen in Figure 40.

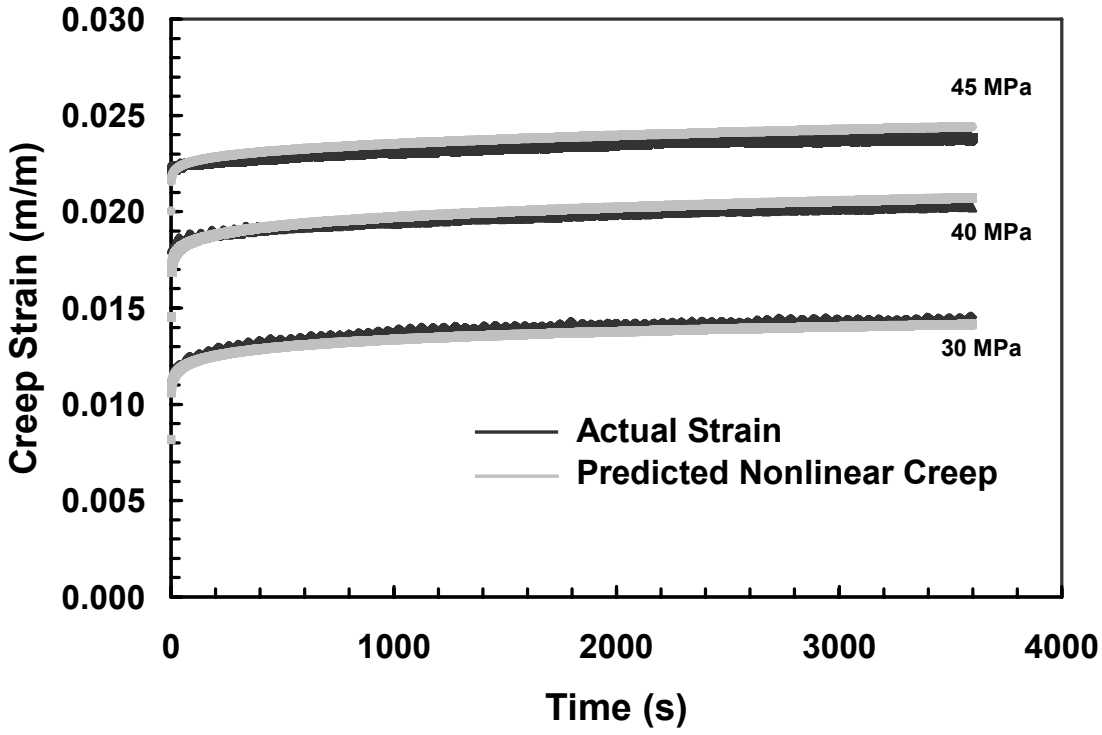

Figure 40. Model predictions for the stepwise creep test

In this scenario, the model performed very well. During the first step, the model slightly under predicts the creep strain. During the next two steps, the model slightly over predicts the creep strain. It appears that the model is capable of predicting creep at higher levels of stress, such as 45 MPa. Therefore the poor prediction of the single step creep test may be due to experimental data scatter. Another bonus was that the model

was able to predict lower creep strain accumulation at 45 MPa compared to that at 30 MPa.

The model predictions were also compared to experimental data obtained in creep tests conducted during unloading (see Figure 41). The model performed well in a sense that it predicted negative creep. Quantitative predictions were also reasonably good for the 40 and 30 MPa tests. However, as can be seen, the prediction became worse as more steps were included. With each step, it took longer for the prediction to approach the experimental values. This is particularly apparent in the case of recovery at zero stress. These results, recorded over a much longer period of time can be seen in Figure 42. Note that 10 h were required for the model prediction to approach the experimental results.

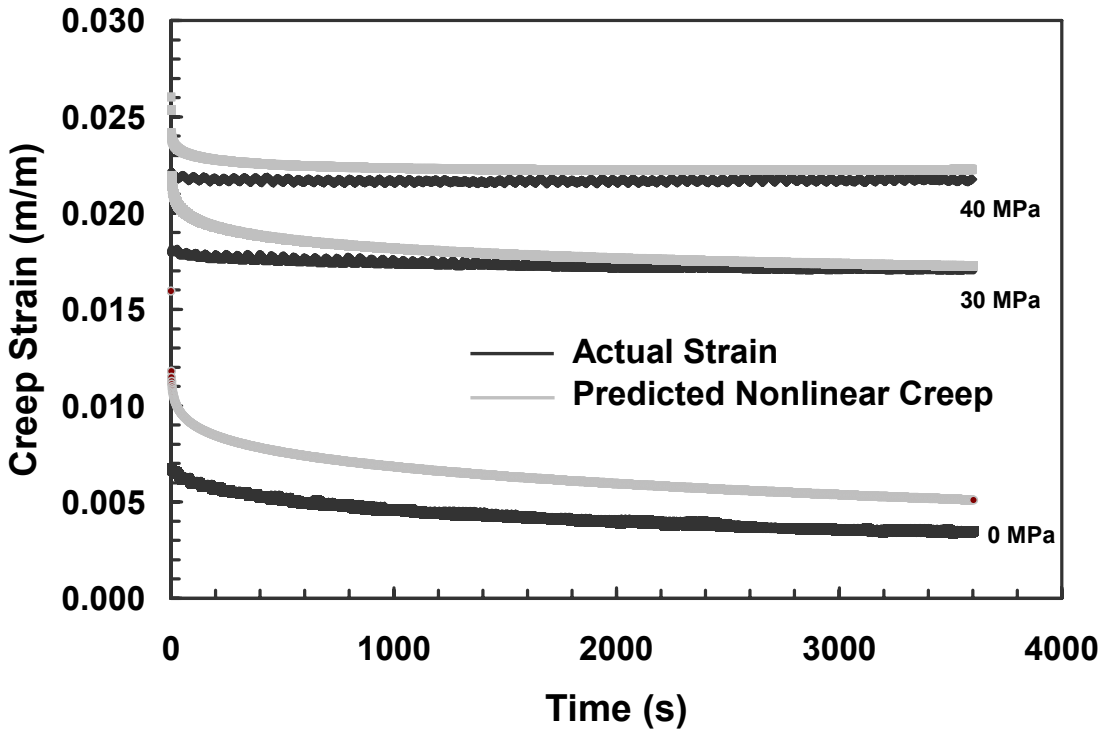

Figure 41. The model predictions for the stepwise creep on the unloading path

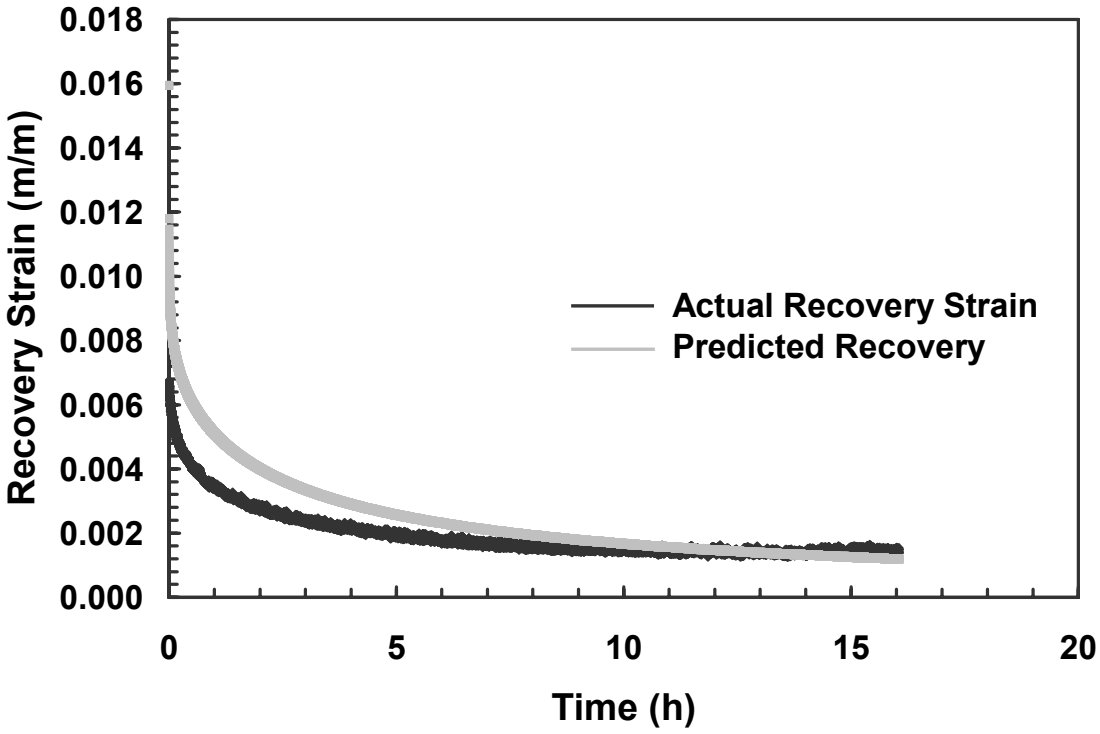

Figure 42. Model Predictions of Recovery at zero stress following the stepwise creep test

VI. Concluding Remarks

Conclusions

This section will wrap up everything that occurred during the testing and explain what their effects were on the BMI 5250-4 neat resin.

Monotonic Behavior

During this section of testing, numerous tests were done to see how the BMI 5250-4 neat resin would react to certain types of loading. They included tests to failure, creep, and recovery tests. Several variables were included to see how they would affect the material. These variables included stress rate and panel variability. During all tests, the thermal expansion and Young's modulus were calculated. The final results gave the following average properties:

Table 8. BMI 5250-4 Properties at 191 °C

Young's Modulus	2.85 GPa
Thermal Expansion	64.56 m/m/ °C

As for the variables, neither the stress rates nor the panels had an effect on the thermal expansion or Young's Modulus. The stress rate did have an effect on both the creep and recovery however. For the fast rate, both creep and recovery (%) were much larger than for the slower stress rate. As for panel variability, it had a drastic effect on the UTS of the material. Between panels, the UTS dropped by nearly 50%. This drop shows the great importance on manufacturing.

Prior History

The prior history on the specimen was studied by performing a stepwise creep test. During this test, the specimen was loaded up to a stress where it could creep for 1 h. After this time, it was loaded to another stress level. There were three levels in all 30, 40, 45 MPa). Once the specimen reached 45 MPa the load steps were reversed to zero in the same manner it was loaded. During this test, the material showed positive creep when preceded by a load up segment and negative creep following an unloading segment. The negative creep was at a smaller magnitude than the positive creep that occurred at that same stress level. It was also shown that both creep and recovery had smaller magnitudes at specific stress values when compared to uninterrupted tests. This test proved that BMI 5250-4 was affected by prior loading history.

Modeling

The model used in this thesis was based on the equation introduced by Schapery. The constants from this equation were determined by performing creep and recovery tests at different stress levels. The tests were performed three times at each stress level to get an average value of the response. To verify the model, predictions were compared to several tests. First, the model was compared to a single step creep test at two different loading rates. For creep preceded by the higher stress rate, there were mixed results. When the stress level was in the range used for model characterization, it performed well. It did not perform well when the stress level was higher than 42 MPa. At the lower stress rate, the model did not accurately predict the creep response because it was not capable of taking into account the slower stress rate. The reason for the better prediction at the higher stress rate was that it compared better to the rate used in determining model parameters.

The third verification test involved the stepwise creep test. The model was able to predict the behavior during every step even the negative creep. However, the accuracy decreased from step to step once the unloading began. Therefore, it was proved that the model could accurately predict creep response of BMI 5250-4 when the prior stress rate is comparable to that used in model characterization.

Recommendations

One of the major points of this research was based on BMI 5250-4 neat resin and how well a nonlinear viscoelastic model could predict its behavior. This topic can be expanded in two ways. First, this material will never be used in the aerospace industry on its own. It will need fiber reinforcement before it can be considered for any application. This introduction will have an effect on all the properties as well as the constants in Schapery's model. It is important to see whether the accuracy of the model will be affected by the fibers. The second possible research topic would include changes in the temperature. In this research, the experiments were isothermal. The Schapery model is capable of making predictions for tests with varying temperatures by the introduction of another constant. This research would give a model for BMI 5250-4 neat resin that has more flexibility in the engineering world.

Bibliography

1. Aklonis, John J. and MacKnight, William J. *Introduction to Polymer Viscoelascticity.* 2nd edition. John Wiley and Sons, 1983

2. Baker, Alan and others. *Composite Materials for Aircraft Structures* (2nd Edition). American Institute of Aeronautics and Astronautics, Inc, 2004.

3. Boyd, Jack D., and Glenn E.C. Chang. "Bismaleimide Composites for Advanced High-Temperature Applications." 38th International SAMPE Symposium, May 10-13, 1993, pp357-363.

4. Cytec Engineered Materials. "CYCOM 5250-4 RTM Resin System." http://www.cytec.com/business/EngineeredMaterials/Datasheets/CYCOM%20RTM%205250-4.pdf.

5. Daniel, Isaac M. and Ori Ishai. *Engineering Mechanics of Composite Materials.* Oxford University Press, 1994.

6. Dowling, Norman E. *Mechanical Behavior of Materials* (2nd Edition). Prentice Hall Publishing, 1999.

7. Eduljee, R.F, J.W Gillespie, Jr, and R.A.Naik. "An Experimental Technique to Characterize the Effect of Through-Thickness Compression on the Interlaminar Shear Response of Composites." The American Institute of Aeronautics and Astronautics, Inc, 1999, pp1427-1431.

8. Elahi, M. and Y.J. Wetisman. *On the Mechanical Response of P4 Chopped Glass/Urethane Resin Composite: Data and Model.* Contract DE-AC05-96OR22464. Oak Ridge, TN: Lockheed Martin Energy Research Corp, October 1999.

9. Findley, William N. and others. *Creep and Relaxation of Nonlinear Viscoelastic Materials.* North Holland Publishing Company, 1976.

10. Jerina, K.L., R.A. Schapery, R.W. Tung, and B.A Sanders. "Viscoelastic Characterization of a Random Fiber Composite Material Employing Micromechanics", *Short Fiber Reinforced Composite Materials, ASTM STP 772,* B.A. Sanders, Ed., American Society for Testing Materials, 1982, pp.225-250.

11. Ju, Jaehyung, and Roger J. Morgan. "Characterization of Microcrack Development in BMI-Carbon Fiber Composite under Stress and Thermal Cycling." *Journal of Composite Materials.* Vol.38, No.22/2004. pp2007-2023.

12. Khan, Fazeel. *The Deformation Behavior of Solid Polymers and Modeling with the Viscoplasticity Theory Based on Overstress.* Rensselaer Polytechnic Institute, Troy, NY, 2002.

13. Krempl, Erhard, and Christine Bordonaro. "A State Variable Model for High Strength Polymers." *Polymer Engineering and Science,* 35: 310-316, (February 1995).

14. Lou, Y.C and R.A Schapery. Viscoelastic Characterization of a Nonlinear Fiber-Reinforced Plastic. *J. Composite Materials,* 5:208-234 (April 1971).

15. Lovell, P. A. and R.J. Young. *Introduction to Polymers* (2nd edition). Chapman and Hall Publishing, 1991.

16. Marks, N. *Polymeric-Based Composite Materials: High Performance Materials in Aerospace.* Edited by Harvey M. Flower. Chapman and Hall Publishing, 1995.

17. MTS Systems Corporation. *Model 793.00 System Software: User Information and Software Reference.* MTS Systems Corporation, 2001.

18. Peretz, D. "Nonlinear Viscoelastic Characterization of FM-73 Adhesive". *Journal of Rheology.* pp245-261. John Wiley & Son, Inc, 1982.

19. Pipkins, A.C, and T.G. Rogers. "A Non-Linear Integral Representation for Viscoelastic Behavior", *J. Mech. Phys. Solids:* 16:59-72 (1968)

20. Raymer, Daniel P. *Aircraft Design: A Conceptual Approach* (3rd edition). American Institute of Aeronautics and Astronautics, Inc., 1999.

21. Riande, Evaristo and others. *Polymer Viscoelasticity: Stress and Strain in Practice.* Marcel Dekker, Inc, 2000.

22. Ruggles, M.B, S. Cheng, E. Krempl. "The Rate- Dependant Mechanical Behavior of Modified 9wt.%Cr-1wt%MO steel at 538ºC," *Materials Science and Engineering*: 15-21 (1994)

23. Ruggles-Wrenn, M.B. Advisor Notes. Air Force Institute of Technology, Wright- Patterson AFB OH, November 2005.

24. Schapery, R.A. On the Characterization of Nonlinear Viscoelastic Materials. *Polymer Engineering and Science.* Vol. 9, No.4: 295-310 (July 1969).

25. Seymoer, Raymond B. *Polymers for Engineering Applications.* ASM International, 1987.

26. Smith, L.V. and Y.J. Weitsman. The Visco-Damage Mechanical Response of Swirl-Mat Composites. *International Journal of Fracture.* 97:301-319 (1999)

27. Ward, I.M, and J. Sweeney. *An Introduction to the Mechanical Properties of Solid Polymers.* John Wiley & Sons, Ltd, 2004.

28. Westberry, Candice, M. *Rate Dependence and Short-Term Creep Behavior of PMR-15 Neat Resin at 23 and 288 °C.* Air Force Institute of Technology, Wright-Patterson AFB OH, September 2005.

REPORT DOCUMENTATION PAGE

Form Approved
OMB No. 074-0188

1. REPORT DATE *(DD-MM-YYYY)*	**2. REPORT TYPE**	**3. DATES COVERED** *(From – To)*
23-03-2006	**Master's Thesis**	Sept 04 – Mar 06

4. TITLE AND SUBTITLE

Some Aspects of the Mechanical Response of BMI 5250-4 Neat Resin at 191 ºC: Experiment and Modeling

5a. CONTRACT NUMBER

5b. GRANT NUMBER

5c. PROGRAM ELEMENT NUMBER

6. AUTHOR(S)

Balaconis, John, G., 2nd Lt, USAF

5d. PROJECT NUMBER
2005-158, 2005-025

5e. TASK NUMBER

5f. WORK UNIT NUMBER

7. PERFORMING ORGANIZATION NAMES(S) AND ADDRESS(S)
Air Force Institute of Technology
Graduate School of Engineering and Management (AFIT/EN)
2950 Hobson Way
WPAFB OH 45433-7765

8. PERFORMING ORGANIZATION REPORT NUMBER

AFIT/GAE/ENY/06-M03

9. SPONSORING/MONITORING AGENCY NAME(S) AND ADDRESS(ES)

AFOSR/NL
Attn: Dr. Charles Y-C Lee
875 Randolph St
Arlington, VA 22203-1954 Comm No: (703)696-7779

AFRL/MLBCM
Attn: Greg Schoeppner
2941 P Street
WPAFB, OH, 45433, (937)255-9072

10. SPONSOR/MONITOR'S ACRONYM(S)

11. SPONSOR/MONITOR'S REPORT NUMBER(S)

12. DISTRIBUTION/AVAILABILITY STATEMENT

APPROVED FOR PUBLIC RELEASE; DISTRIBUTION UNLIMITED.

13. SUPPLEMENTARY NOTES

14. ABSTRACT

The mechanical response of BMI 5250-4 neat resin at 191ºC was studied using both creep and recovery tests where several variables were allowed to change. In these tests, the effect of stress rate, prior history, and panel variability were all taken into account. During the creep test, the material showed both primary and secondary creep over 20 h. The recovery tests showed full recovery after it was subjected to 80% UTS. The higher stress rate caused a much greater response in both creep and recovery tests. The prior history was studied by allowing the specimens to go through a stepwise creep test. They behaved similar to the single step creep test when preceded by a loading segment. During creep tests preceded by unloading, the material showed a decrease in creep strain. This decrease grew as the creep stress approached zero. The only difference that could be seen with panel variability was that the UTS dropped dramatically between the panels.

A nonlinear viscoelastic model was created that was based on the work by Schapery. This model included four constants that were material specific and stress dependant. These constants were obtained by viewing the response during a two- step program including creep and recovery. The model was verified by comparing the predictions to previous tests including the creep and stepwise creep tests. The model predicted the creep strain preceded by load up well. It was capable of showing the response of the negative creep but the error grew as more steps were introduced. The model could not take into account stress rate. Therefore it could only predict the results at the higher stress rate.

15. SUBJECT TERMS

Polymer, BMI 5250-4, creep, recovery, prior stress rate, prior loading history, nonlinear viscoelastic theory

16. SECURITY CLASSIFICATION OF:			**17. LIMITATION OF ABSTRACT**	**18. NUMBER OF PAGES**	**19a. NAME OF RESPONSIBLE PERSON**
REPORT	**ABSTRACT**	**c. THIS PAGE**			Dr. Marina B. Ruggles-Wrenn
U	**U**	**U**	**UU**	94	**19b. TELEPHONE NUMBER** *(Include area code)* 785-3636, ext 4641; e-mail: @afit.edu

Standard Form 298 (Rev: 8-98)
Prescribed by ANSI Std. Z39-18